CHAPTER 19

LOW ENERGY ELECTRON DAMAGE TO DNA

LÉON SANCHE*

Groupe en Sciences des Radiations, Département de médecine nucléaire et de radiobiologie, Faculté de médecine, Université de Sherbrooke, Québec, Canada J1H 5N4

Abstract: The results of experiments, which measured the damage induced by the impact of low energy electrons (LEE) on DNA under ultra-high vacuum conditions, are reviewed with emphasis on transient anion formation. The experiments are briefly described and several examples are presented from results on the yields of fragments produced as a function of the incident energy (0.1–30 eV) of the electrons. By comparing the results from experiments with different forms of the DNA molecule (i.e., from short single stranded DNA having four bases to plasmids involving $\sim 3,000$ base pairs) and theory, it is possible to determine fundamental mechanisms that are involved in the dissociation of basic DNA components, base release and the production of single, double-strand breaks and cross-links. Below 15 eV, electron resonances (i.e., the formation of transient anions) play a dominant role in the fragmentation of any bonds within DNA. These transient anions modify or fragment DNA by decaying into dissociative electronically excited states or by dissociating into a stable anion and a neutral radical. The fragments can initiate further reactions within DNA and thus cause more complex chemical damage. The incident electron wave can first diffract within the molecule before temporary localization on a basic DNA unit, but when transient anion decay by electron emission occurs, the departing electron wave can also be strongly enhanced by constructive interference within the DNA molecule. The experiments with oligonucleotides reported in this article show that the amount of damage generated by 3–15 eV electrons is dependent on base identity, base sequence and electron energy. Capture of a LEE by a DNA subunit may also be followed by electron transfer to another. Such transfers are affected by base stacking and sequence. Furthermore, the damage is strongly dependent on the topology and environment of DNA and the type of counter ion on the phosphate group. In particular, condensing H2O on a DNA induces the formation of a new type of transient anion whose parent is a H2O-DNA complex. Finally, under identical conditions, LEE were found to be three times more effective than X rays to produce strand breaks

Keywords: Electrons, DNA, Radiation Damage, Anion Desorption, Dissociative Attachment, Strand Breaks

* Corresponding author, e-mail: Leon.Sanche@USherbrooke.ca

M. K. Shukla, J. Leszczynski (eds.), Radiation Induced Molecular Phenomena in Nucleic Acids, 531–575.

19.1. INTRODUCTION

Many investigations during the past century have been devoted to the understanding of the alterations induced by high energy radiation in biological systems, particularly within living cells and to the DNA molecule. The biological effects of such radiation are not produced by the mere impact of the primary quanta, but rather, by the secondary species generated along the radiation track [1]. As these species further react within irradiated cells, they can cause mutagenic, genotoxic and other potentially lethal DNA lesions [2–5], such as base and sugar modifications, base release, single strand breaks (SSB), and cluster lesions, which includes a combination of two single modifications, e.g. double strand breaks (DSB) and cross-links [2, 3, 5, 6]. Secondary electrons (SE) are the most abundant of the secondary species produced by the primary interaction [7–9]. For example, a 1 MeV primary photon or electron generates about 3×10^4 SE of low energy ($E < 30$ eV), when its energy is deposited in biological matter [7, 8, 10]. Once created, such low energy electrons (LEE) produce large quantities of highly reactive radicals, cations and anions. These reactive species produce new compounds and damage biomolecules within irradiated cells. In the vicinity of cellular DNA, these species arise from DNA itself, water and other biomolecules in close contact with that molecule such as histone proteins. Thus, LEE either damage DNA directly or via the species they produced. It is therefore crucial to determine the action of LEE within cells, particularly in DNA where they could induce genotoxic damage.

In order to understand the basic mechanisms involved in LEE-induced damage in DNA both experimentalists and theoreticians have adopted a systematic approach to the problem by investigating LEE interactions with molecules of increasing complexity; i.e., with isolated basic constituents of DNA (the base, phosphate, sugar and water subunits), with a number of these constituents bonded together and with the entire molecule [5]. According to this approach, future investigations should be performed with DNA embedded in more complex environments containing water, oxygen and proteins so as to learn how the fundamental electron-DNA interactions are modified in the cellular medium and to determine the damage produced by species created around DNA by LEE. Such research has been initiated in many calculations on electron attachment to di-nucleotides, or shorter strands of DNA, where these latter have been embedded in a continuously polarizable medium representing water [11–15]. In a recent article, the author has reviewed the experimental and theoretical results obtained from nucleotides, nucleosides and basic DNA constituents both in the gas and the solid phase [5]. Theoretical advances, which occurred since this last review, are discussed in other chapters of this book. The present article is limited to a review of the experimental results obtained from LEE impact experiments on single and double stranded DNA. Some theoretical results are mentioned in relation with those from experiments. The most useful techniques to analyze the damage produced by LEE to DNA are described in Section 19.2. The experimental results obtained with this molecule are presented and discussed in Sections 19.3 to 19.6 ; the conclusions are given in Section 19.7.

19.2. EXPERIMENTAL METHODS

19.2.1. Deposition of Thin DNA Films

The DNA molecule consists [16] of two polynucleotide antiparallel strands having the form of a right-handed helix. Depending on the genetic information encoded within the molecule, it may contain thousands up to billions of atoms (mostly hydrogen and carbon). Within DNA, the strands are composed of repeated sugar-phosphate units hydrogen bonded together through the four fundamental bases, which are covalently linked to the sugar moiety of the backbone. This is illustrated in Figure 19-1 for a short double-stranded segment. It consists of two sets of sugar rings with the bases guanine (G) and adenine (A), hydrogen bonded to cytosine (C) and thymine (T), respectively. With such a complex and massive molecule, LEE investigations must be performed in the condensed phase, on thin films grown on a conductive substrate, so as to avoid charging of the surface by the incident electrons. When deposited in ultra-high vacuum (UHV) as a thin film condensed on a substrate, DNA still contains on average 2.5 water molecules per nucleotide [17]. These H_2O molecules, which easily fit in the grooves of the helix, are an integral part of the DNA structure. The negative charge on one of the oxygens of the phosphate group is counterbalanced by a cation. The nature of this latter depends on the buffer used in the procedure to prepare a solution of DNA (i.e., Na^+ if the buffer is NaCl). In B-type DNA, the crystallographic (averaged) structure resembles that of a twisted ladder with base pairs defining the rungs and the backbone providing the side support. The helical pitch, that is, the distance for a full turn of the helix, is 3.4 nm and there are 10 rungs per turn. The base pairs lie in a plane perpendicular to the helix axis. In A-type DNA, however, the vertical stacking is appreciably smaller. There are 11 base pairs per turn and the pitch is 2.8 nm. Moreover, in the A-type there is an important tilt of 20° of the plane of the base pairs with respect to the helix axis. In the cell, DNA is in the B form, whereas in its dried state the molecule adapts the A configuration [16].

For compounds that might be decomposed by sublimation into vacuum, such as DNA, two different techniques have been developed to produce thin biomolecular films on metal substrates. When multilayer films are required, the molecules are put in a solution from which a small aliquot is lyophilized on a tantalum substrate [18]. The sample preparation and manipulations are performed within a sealed glove box under a pure dry nitrogen atmosphere. The average film thickness is usually estimated from the amount of biomolecular material deposited and its density [18]. Relatively thick ($\sim$ 5 monolayers: ML) films are prepared to insure that the measured signal arises from electron interaction with biomolecules that lie close to the film-vacuum interface.

When only a single layer of DNA is needed, a uniform and clean layer can be chemisorbed on a gold substrate by the technique utilized to prepare self-assembled monolayers (SAM) [19, 20]. The gold substrate is usually prepared by vacuum evaporation of high-purity gold (99.9%) onto freshly cleaved preheated mica slides [20]. These slides are dipped for at least 24 h in an aqueous solution of highly

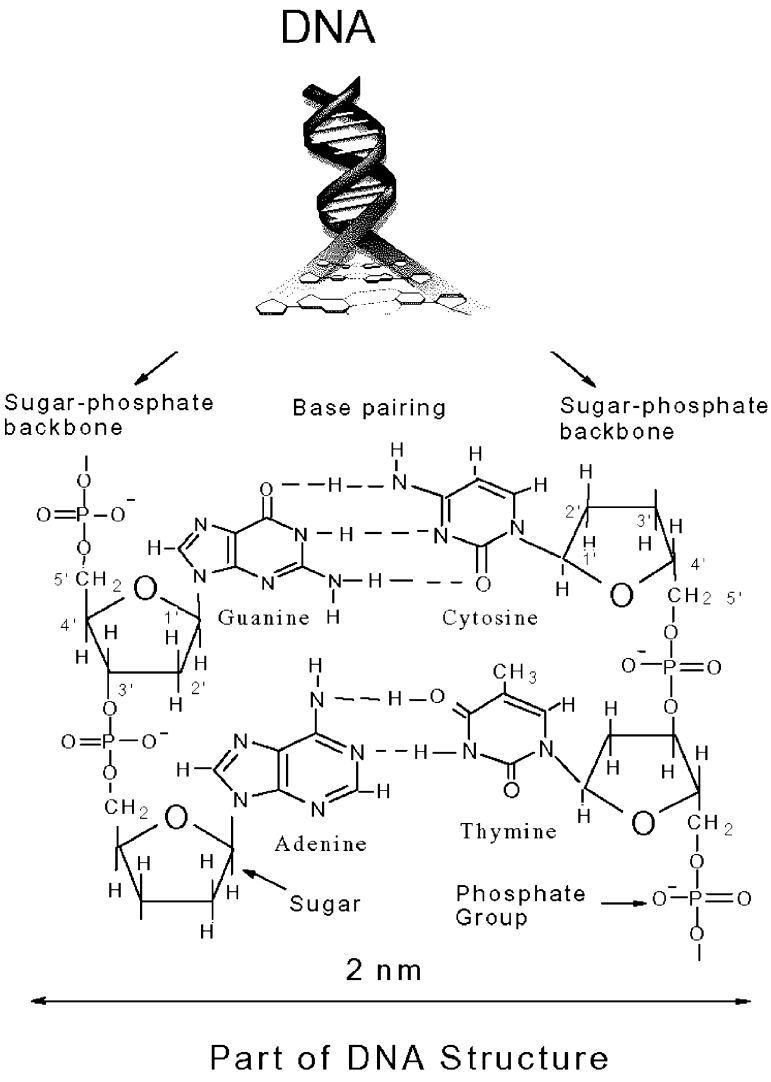

Figure 19-1. Segment of DNA containing the four bases

purified DNA. After removal of the mica-Au-oligo slide from the solution, it is rinsed with a copious amount of nanopure water and dried under nitrogen flow. Each slide is divided into smaller samples, which are afterwards mounted on a multiple sample holder, such as that shown in Figure 19-2. With this procedure, one monolayer [20, 21] is chemically anchored to the gold substrate via a phosphothioate modification on one or many nucleotides (i.e., substitution of the double-bonded oxygen atoms by double-bonded sulfur at the phosphorus). Considering that the

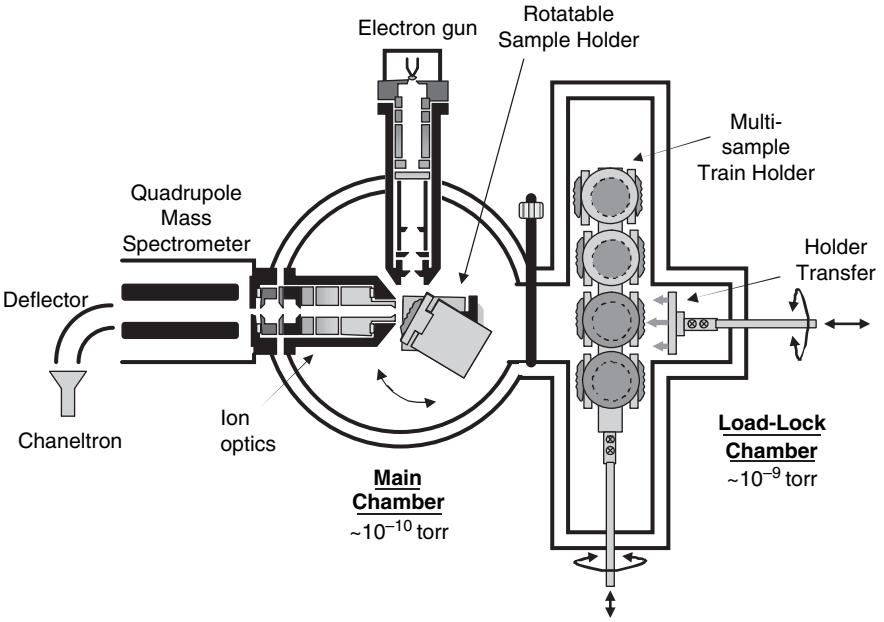

Figure 19-2. Schematic overview of the type of apparatus used to investigate the desorption of ions and neutral species induced by electron impact on thin molecular and bio-organic films. In the case of thin DNA films, they are formed outside vacuum by lyophilization on a metal substrate or as a self-assembled layer. The films are placed on the multi-sample holder in the load-lock chamber. From there, they can be transferred one by one to the main chamber for analysis

chemisorbed oligos are well ordered and densely packed, an upper limit for the surface coverage (i.e., $N_0 \approx 1.7 \times 10^{14}$ oligos/cm^2) [22] is obtained, regardless of the nature and number of the bases. The reproducibility of the results obtained so far [20–22] suggests that the surface coverage can be estimated within an error of 20%.

19.2.2. Electron Bombardment

Once prepared, the DNA samples are placed either directly into an UHV chamber or into a load lock UHV chamber. A schematic diagram of a system having a load-lock chamber is shown in Figure 19-2. The load-lock chamber ($\sim 2 \times 10^{-9}$ torr) is equipped with a multi-sample holder, to which 16 samples can be mounted and individually transported into a rotary target holder in the main chamber ($\sim 1 \times 10^{-10}$ torr). In this chamber, an electron source consisting of a modified LEE gun is focused on a 2 mm^2 spot onto the target. The energy distribution of the electrons emitted from the gun is approximately 0.4 eV full width at half maximum (FWHM) with a beam current adjustable between 1nA and 1 μA [23]. Electrons from 0.1 to 100 eV impinge onto the sample at an incident angle of 70° with respect to

the surface normal. The electron energy scale is calibrated by taking 0 eV as the onset of electron transmission through the film, with an estimated uncertainty of ± 0.3 eV [24]. Because energy shifts in this onset are related to electron trapping, this calibration method allows one to verify that measurements are obtained from uncharged films; alternatively, with this method it is possible to obtain an estimate of charge accumulation during electron impact [25]. To avoid charging the films with the electron beam, its thickness must be smaller than the effective range (12–14 nm) for damaging DNA with LEE [18] and the penetration depth of 5–30 eV electrons (15–30 nm in liquid water or amorphous ice) [26]. Under these conditions, most of the electrons from the beam are transmitted through the DNA film under single inelastic scattering conditions.

Other types of electron sources, such as SE emitted from metal substrates, can be used to irradiate DNA samples [6]. When a sufficiently thin (< 5 nm) biomolecular film deposited on a metal substrate is exposed to X-ray photons; these latter are not appreciably absorbed by the film. Under these conditions, the induced damage may be considered to result from electrons emitted from the substrate with the energies of the measured SE distribution. The latter is usually broad but contains essentially LEE. For example, the energy spectrum of $Al_{k\alpha}$ X-ray induced SE emission from tantalum has a peak at 1.4 eV and an average energy of 5.8 eV [6].

Another possibility is to use a defocused LEE beam to irradiate large quantities of non-volatile organic and biological molecules, spread out over a large surface area. In such an irradiator, recently developed by Zheng et al. [27], the molecules under investigation are spin coated onto the inner surface of tantalum cylinders. Up to ten cylinders can be placed on a rotary platform housed in an UHV system, where their inner walls are bombarded by a diverging beam of electrons having an energy distribution of 0.5 eV FWHM. The electrons first reach a cylindrical mesh grid and then are accelerated to any desired energy by a voltage applied between the grid and the cylinder. The uniformity of the incident electron current over the inner wall of the cylinders is adjusted by inserting the electron gun and grid into a stack of 12 ring current detectors. After irradiation, the cylinders are removed from UHV and the samples are dissolved in an appropriate solvent. With this type of irradiator, the amount of molecules that can be irradiated by LEE in a single bombardment period is about two orders of magnitude higher than that with a conventional electron gun.

19.2.3. Electron-Stimulated Desorption (ESD) of Ions and Neutral Species

As shown in Figure 19-2, neutral and ionic species desorbing from a biomolecular film can be analyzed by mass spectrometry. Whereas ions that emerge from the film can be focused by electrostatic lenses located in front of the mass spectrometer (MS), neutral species spread in all directions. So, to obtain reasonable signals for the desorbing neutral species, they are usually ionized close to the target surface by a laser [28] and then the resulting ions focused into the MS (i.e., in the example

of Figure 19-2, into quadrupole rods). However, in order to determine the absolute desorption yields of neutral products, their formation must be related to a pressure rise within a relatively small volume. In this case, a MS measures in a small UHV chamber the partial-pressure increase due to the desorption of a specific fragment induced by LEE impact on a thin film [20–22]. At equilibrium, the number of fragments desorbed per unit time, $N_d/\Delta t$, is equal to the relative partial pressure variation, ΔRPP, times a factor of 1.3×10^{18} that corresponds to SN/RT, where S is the true nominal pumping speed of the system, N is Avogadro's number, R is the perfect gas constant, and T is the temperature [22]. The effective number of a specific fragment desorbed per incident electron is proportional to the effective desorption cross-section via the constant (N_0/a), where N_0 is the initial number of target molecules in the irradiated area a [22, 29].

In certain systems, grids are inserted between the electrostatic lenses in order to analyze the ion energies by the retarding potential method. Relative ion yields can be obtained from three different operating modes [30]: (1) the ion-yield mode, in which the ion current at a selected mass is monitored as a function of incident electron energy, (2) the ion-energy mode, in which the same latter current is measured for a fixed electron energy as a function of the retarding potential, and (3) the standard mass mode, in which a mass spectrum over a selected range is recorded for a fixed electron energy.

19.2.4. Analysis by Electrophoresis and High Performance Liquid Chromatography (HPLC)

Once extracted from the UHV system, the irradiated samples can, in principle, be identified by various standard methods of chemical analysis. However, the quantity of recovered material and fragments produced by the type of apparatus shown in Figure 19-2 are so small that an efficient method of damage amplification is required to observe any type of fragmentation. One method of damage amplification consists of using as a target film plasmid DNA, in which a small modification at the molecular level can cause a large conformal change. A single bond rupture in the backbone of a plasmid of a few thousand base pairs can cause a conformational change in the geometry of DNA, and hence be detected efficiently by agarose gel electrophoresis, after bombardment by a focused LEE beam. The product in each electrophoresis band can be quantitated and identified as cross links (CL), supercoiled (undamaged), nicked circle, corresponding to SSB and full-length linear, corresponding to DSB or short linear forms [18, 31]. The procedure can be repeated at different electron energies and irradiation times.

Such a huge amplification factor does not exist for other DNA damages that do not involve strand breaks and CL. In this case, the quantity of fragments produced from a collimated electron beam is not sufficient for chemical analysis. To produce sufficient degraded material the new type of LEE irradiator described in the Section 19.2.2 can be used to bombard much more material. This technique allows the total mixture of products resulting from LEE bombardment of DNA to be

analyzed by HPLC/UV and gas chromatography/MS. When analysis is performed only by HPLC, the identification of the products and their yields is determined by calibration with authentic reference compounds.

19.3. INTERPRETATION OF THE DEPENDENCE OF FRAGMENT YIELDS ON INCIDENT ELECTRON ENERGY

To interpret in terms of fundamental processes the incident energy dependence of the production of fragments (i.e., the yield functions) induced by LEE impact on DNA films, some knowledge of the interaction between an electron and a molecule is required. In general, the interaction of an electron with an atom or a molecule can be described in terms of forces derived from the potential acting between them. At low energies (0–30 eV), there are basically three types of forces that act between an electron and a molecule [32]: (1) the electrostatic force; (2) the exchange force, which reflects the requirement that the electron-target system wave function must be antisymmetric under pairwise electron exchange; and (3) the induced polarization attraction, which is due to the distortion of the target orbitals by the electric field of the projectile electron. At certain energies, these forces may combine to produce an effective potential capable of momentarily capturing the scattering electron. This "resonance" phenomenon causes the formation of a transient anion [33].

The electron-molecule interaction in the range 1–30 eV can therefore be described in terms of resonant and non-resonant or direct scattering. The latter occurs at all energies above the energy threshold for the observed phenomenon, because the potential interaction is always present. Thus, direct scattering produces a smooth usually rising signal that does not exhibit any particular features in low-energy yield functions. In counterpart, resonance scattering occurs only when the incoming electron occupies a previously unfilled orbital, which exists at a precise energy [34, 35], and thus correspond to the formation of a transient anion. At the resonance energy the formation of a product is usually enhanced. The dependence of the yield of DNA fragments and the desorbed ion and neutral yields on incident electron energy is, thus, expected to exhibit pronounced maxima superimposed on an increasing monotonic background from direct scattering.

Electron resonances are well-described in the literature and many reviews contain information relevant to this scattering phenomenon [30, 33–39]. There are two major types of electron resonances or transient anions [33]. If the additional electron occupies a previously unfilled orbital of the target in its ground state, then the transitory anion state is referred to as "shape" or single-particle resonance. The term "shape" indicates that the electron trapping is due to the shape of the electron-molecule potential. When the transitory anion involves two electrons that occupy previously unfilled orbitals, this transitory state is referred to as "core-excited" or two-particle, one-hole resonance. In principle, such resonances may lie below or above the energy of their parent neutral state. The former case, where the incoming electron is captured essentially by the electron affinity of an electronically excited state of the molecule, corresponds to a Feshbach type resonance. The latter case, where the capture is aided by the angular momentum barrier from the

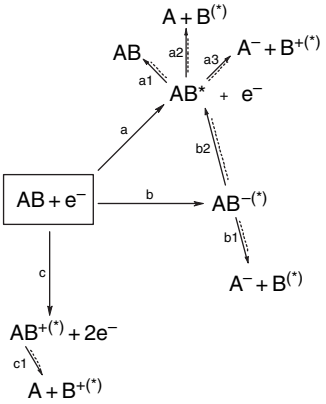

Figure 19-3. Unimolecular fragmentation pathways that follow low-energy electron interaction with a diatomic molecule AB. The asterisk in parentheses indicates that the species could be electronically excited. (Reprinted with permission from [21]. Copyright 2000 American Chemical Society.)

non-zero momentum partial wave content of the attaching electron, is called a core-excited shape resonance.

For a simple molecular liquid or solid composed of diatomic molecules AB, unimolecular fragmentation pathways at low energies are described in Figure 19-3. The direct electron interaction may produce an excited neutral state of the molecule (AB^*) via pathway a. AB^* may slowly dissipate its excess energy via photon emission and/or energy transfer to the surrounding medium (i.e., a1). If the configuration of an electronic excited state is dissociative, then AB^* may quickly fragment into two atoms (or neutral radicals in the case of a more complex molecule) as shown by the a2 pathway. Above a certain energy threshold (~14–16 eV), fragmentation may occur via dipolar dissociation (DD), path a3, to gives an anion and a cation. In the case of resonant scattering, the b pathway, the resulting transient anion may autoionize via b2 or, for a sufficiently long-lived anion in a dissociative state, it may fragment into a stable anion and a neutral atom or radical via b1. This latter mechanism is known as dissociative electron attachment (DEA). When the $(AB^-)^*$ state lies above of its parent, AB can be electronically excited after electron detachment (b2); in this case, it can decay into the a1, a2, or a3 pathways previously described. Finally, the incoming electron can directly ionize the molecule via path c, and if the resulting cation is dissociative, then it may fragment, as shown by reaction c1. This dissociation channel is usually non-resonant.

19.4. PLASMID DNA

Plasmid DNA was first bombarded with electrons of energies lower than 100 eV by Folkard et al. [40] who found threshold energies for SSB and DSB at 25 and 50 eV, respectively. Later, Boudaiffa et al. bombarded with 5 eV to 1.5 keV electrons dry samples of pGEM®-3Zf(-) plasmid DNA films [31, 41–43]. Their samples

were analyzed by electrophoresis to measure the production of circular and linear forms of DNA corresponding to SSB and DSB, respectively. By measuring the relative quantities of these forms in their 5-ML sample as a function of exposure to electrons, these authors obtained the total effective cross-section ($\sim 4 \times 10^{-15}$ cm^2) and effective range (~ 13 nm) for the lost of supercoiled DNA, at 10, 30, and 50 eV [18]. Such experiments also allowed Boudaiffa et al. to delineate the regime under which the measured yields were linear with electron exposure. It is within this regime that the incident electron energy dependence of damage to DNA was recorded more continuously between 5 and 100 eV [31, 41, 42]. Figure 19-4 shows the measured yields of SSB and DSB induced by 5–100 eV electrons. At each electron energy, the error bar in Figure 19-4 corresponds to the standard deviation of the average reported value.

Whereas the DSB yield begins near 6 eV, the apparent SSB yield threshold near 4–5 eV is due to the cut-off of the electron beam at low energies. Both yield functions have a peak around 10 eV, a pronounced minimum near 14–15 eV followed by an increase between 15 and 30 eV, and a roughly constant yield up to 100 eV. From the explanations of the previous Section 19.3, it becomes obvious that the SSB and DSB yield functions can be divided into two regimes. One below 15 eV, where the electron DNA interaction occurs essentially via electron resonances and another regime above 15 eV, where as shown by the dotted line, the yield increases

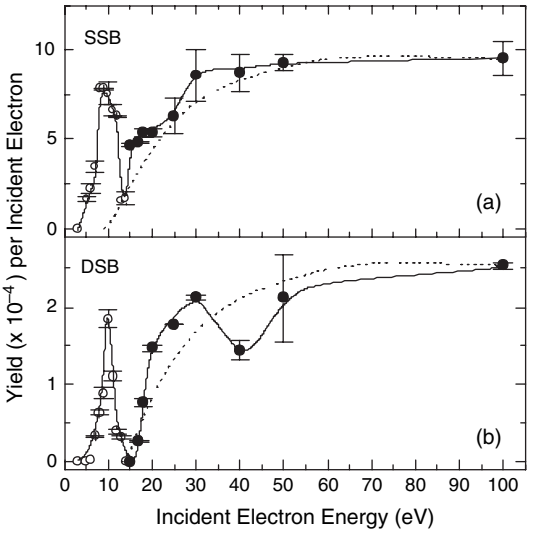

Figure 19-4. Open and solid symbols are the measured quantum yields (events per incident electron) for the induction of single strand breaks (SSB) (a) and double strand breaks (DSB) (b) in DNA films by 4–100 eV electron impact. The solid curves through the data are guides to the eye. The dotted curves symbolize general electron energy dependence of the cross sections for various nonresonant damage mechanisms, such as ionization cross sections, normalized here to the measured strand break yields at 100 eV

monotonically and saturates above 50 eV. This latter behavior is characteristic of direct scattering, with superposition of broad resonances between 20 and 40 eV.

The resonances in the yield functions of SSB and DSB appear more clearly in Figure 19-5. The major peak near 10 eV now appears as a superposition of broad resonances at different energies. These yield functions can be understood from the results of the fragmentation induced by LEE to the various subunits of the DNA molecule, including its structural water. In fact, the strong energy dependence of DNA strand breaks below 15 eV can be attributed to the initial formation of transient anions of specific DNA subunits decaying into the DEA and/or dissociative electronic excitation channels, as exemplified in Figure 19-3. However, because the DNA subunits, which include the phosphate, sugar, base and structural H_2O, can all be fragmented via DEA between 5 and 13 eV, it was not possible, without more detailed investigation, to unambiguously specify the component responsible for SSB and DSB.

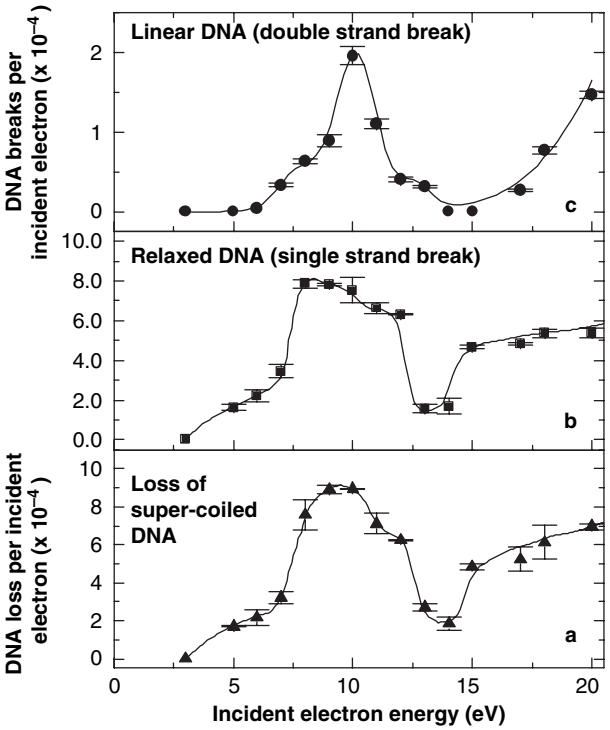

Figure 19-5. Measured yields, per incident electron of 5–20 eV, for the loss of the supercoiled DNA form (a), induction of SSBs (b), and DSBs (c) in dry DNA films. The error bars correspond to one standard deviation from six measurements. (Reprinted with permission from [31]. Copyright 2000 American Association for the Advancement of Science.)

Since the data in Figure 19-5 was recorded in the linear regime with electron exposure, each SSB or DSB is the result of a single electron interaction. To explain the induction of two strand breaks by single electron, it has been suggested that below ~ 16 eV, DSB occurs via molecular dissociation on one strand initiated by the decay of a transient anion, followed by reaction of at least one of the fragmentation products on the opposite strand [31, 41]. This hypothesis was supported by experiments in condensed films that contain water or molecular oxygen mixed with small linear and cyclic hydrocarbons [44–46]. In such films, electron-initiated fragment reactions (such as hydrogen abstraction, dissociative charge transfer and reactive scattering) were found to occur over distances comparable to the DNA double-strand diameter (~ 2 nm).

A more precise interpretation of DNA damage below 15 eV came from the experiments of Pan et al. [47], who directly measured ESD of anions from plasmid and 40 base-pair synthetic DNA within the 3–20 eV range. Resonant structures were observed with maxima at 9.4 ± 0.3, 9.2 ± 0.3, and 9.2 ± 0.3 eV, in the yield functions of H^-, O^-, and OH^-, respectively. The yield function for H^- desorption, from synthetic and plasmid double stranded DNA is shown in Figure 19-6A and 6B, respectively. The yield functions for O^- and OH^- desorption exhibit a similar behavior. The prominent 9 eV feature observed in all anion yield functions is a typical signature of the DEA process. The maxima in the H^-, O^- and OH^- yield functions from DNA can be correlated with the maximum seen between 8 eV to 10 eV in the SSB yield and the one occurring at 10 eV in the DSB yield induced by LEE impact on films of supercoiled DNA in Figure 19-5 [31, 42]. Curves C, D and E in Figure 19-6 represent the yield functions for the desorption of H^- from films of thymine [48], amorphous ice [49], and α-tetrahydrofuryl alcohol [50]. The results obtained for the three other bases are similar to that shown for thymine [48]. Those obtained from THF and other DNA backbone sugar-like analogs [50] are essentially the same as the curve E in Figure 19-6. The H^- peak from amorphous water in D is too weak to be associated with DEA to the structural water of DNA. It is also found near 7 eV, an energy too low to be associated with the H^- peak from DNA, unless the strong hydrogen bonding in DNA [4] shifts considerably the H_2O^- resonance to higher energy. In contrast, comparison of curve C with curves A and B in Figure 19-6 indicates that the bases are an important source of desorbed H^- with intensity about 3 times larger than the one arising from the sugar ring (curve E). A similar conclusion can be reached from comparison with gas-phase H^-/D^- abstraction from the carbon position in thymine [51]. Hence, comparison of line shapes and magnitude of the yield functions in both phases suggests that LEE-induced H^- desorption from DNA below 15 eV occurs mainly via DEA to the bases with a possible contribution from the deoxyribose ring.

Similar comparisons between the anion yield functions from basic DNA constituents and those of O^- and OH^- from DNA films [47] indicate that O^- production arises from temporary electron localization on the phosphate group. The yield function for OH^- desorption resembles that of O^-, but has a lower

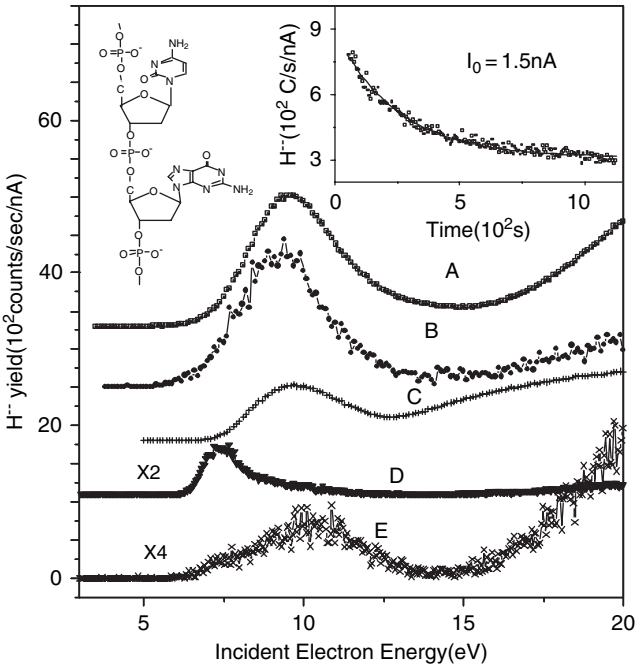

Figure 19-6. The H^- yield function from thin films of: (A) double stranded linear DNA, 40 base-pairs, (B) supercoiled plasmid DNA, (C) thymine, (D) ice, and (E) a deoxyribose analog. The zero-count baseline of curves A-D has been displaced for clarity. Part of a single DNA strand is shown in the left corner at the top. The dependence of the magnitude of the H^- signal from DNA on time of exposure to the electron beam is shown in the insert

intensity. As explained in Section 19.5, detailed analysis of SAM of DNA indicates that OH^- signal arises also from the phosphate group when the counter ion is a proton.

It was only after the development of more efficient techniques to purify DNA that the electron energy range below 4 eV was investigated by Martin et al. [52]. *The increase in sensitivity of DNA to LEE damage allowed the use of electron current of only* 2.0 *nA and exposure times shorter than* 20 *seconds to irradiate the samples of plasmid DNA*. Under these conditions, the 0.1–5 eV range was explored without beam defocusing and film charging. As in previous experiments, the different forms of DNA were separated by gel electrophoresis and the percentage of each form was quantified by fluorescence. Exposure response curves were obtained for several incident electron energies. As an example, the inset of Figure 19-7 shows the dependence of the percentage yields of circular DNA on irradiation time for 0.6 eV electrons. Since, the amount of the linear form of plasmid DNA was below the detection limit of 0.2 nanograms between 0.1 and 4 eV, DSB were considered not to be formed below 5 eV. The yields of SSB per incident electron were determined from the amounts of circular DNA resulting from a 10 s exposure.

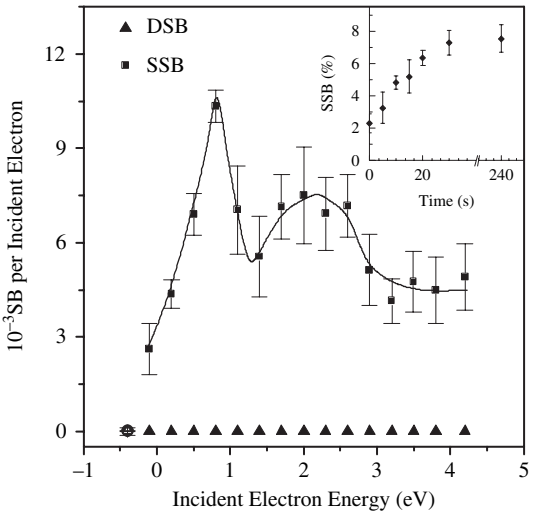

Figure 19-7. Yields of SSBs and DSBs induced by 0–4.2 eV electrons on supercoiled plasmid DNA films. The inset shows the dependence of the percentage of circular DNA (i.e. SSB) on irradiation time for a beam of 0.6 eV electrons of 2 nA

Two peaks, with maxima of $(1.0 \pm 0.1) \times 10^{-2}$ and $(7.5 \pm 1.5) \times 10^{-3}$ SSB per incident electron are seen in Figure 19-7 at electron energies of 0.8 eV and 2.2 eV, respectively. The error bars in the yield function show the standard deviation from 3 to 8 exposure experiments, each on separately prepared samples. *These peaks provide unequivocal evidence for the role of shape resonances in the bond breaking process.* Martin et al. [52] compared these results with those from the basic DNA units. The solid curve in Figure 19-7, which reproduces in magnitude and line shape the yield function, was obtained by a model that simulates the electron capture cross section as it might appear in DNA owing to the π^* single-particle anion states of the bases. The attachment energies were taken from the transmission measurements [53] and the peak magnitudes were scaled to reflect the inverse energy dependence of the electron capture cross sections. Assuming an equal numbers of each base in DNA, the contributions from each base were simply added. The lowest peak in the modeled capture cross section, which occurs at 0.39 eV in the gas phase, was shifted by 0.41 eV at higher energy to match that in the SSB yield and its magnitude normalized. The relationship between the resonances in the bases and SSB in DNA offered support for the charge transfer mechanism of Barrios et al [11], meaning that an anionic potential energy surface connects the initial π^* anion state of the base to a dissociative σ^* anion state of the phosphate group.

Following these observations, Panajotovic et al. [54] determined effective cross sections for production of SSB in plasmid DNA [pGEM 3Zf(-)] by electrons of 10 eV and energies between 0.1 and 4.7 eV. The effective cross sections were derived from the slope of curve of the yield *vs* exposure in the linear regime.

They reported values in the range of 10^{-15}–10^{-14} cm^2, which translate into effective cross sections of the order of 10^{-18} cm^2 per nucleotide. The cross sections within the 0–4 eV range were similar in magnitude to those found at higher energies (10–100 eV) indicating that the sensitivity of DNA to electron impact is universal and not limited to any particular energy range.

It is difficult to compare directly the yields obtained by LEE impact under UHV conditions, with those obtained from experiments in which DNA or other biomolecules are irradiated by high energy particles, mainly because of different experimental conditions, including the composition and conformation of the DNA. In addition, the dosimetry for LEE beam experiments is not available due to problems related to the energy imparted both to the DNA film and the metal substrate [42, 43]. By using an X-ray SE emission source as described in Section 19.2.2, Cai et al. [6] were able to compare directly DNA damage induced by high-energy photons ($Al_{k\alpha}$X-rays of 1.5 keV) and LEE under almost identical experimental conditions. In their experiments, both monolayer and thick (20 μm) films of dry plasmid DNA deposited on a tantalum foil were exposed to 1.5 keV X-rays for various times in an UHV chamber. In the monolayer case, the damage was induced mainly by the low energy SE emitted from tantalum. For the thick films, DNA damage was induced chiefly by X-ray photons. Different forms of plasmid DNA were separated and quantified by agarose gel electrophoresis. The exposure curves for the production of SSB, DSB, and interduplex CL were obtained for both monolayer and thick films of DNA. The lower limits of G values for SSB and DSB induced by SE were derived to be 86 ± 2 and 8 ± 2 nmol J^{-1}, respectively. *The average G values were about* 2.9 *and* 3.0 *times larger, respectively, than those obtained with* 1.5 *keV photons* [6].

Later Cai et al. [55] performed similar experiments in air. They investigated similar thick and thin films of pGEM®-3Zf(-) plasmid DNA deposited on a tantalum foil with soft X-rays of 14.8 keV effective energy for different times under relative humidity of 45% ($\Gamma \approx 6$, where Γ is the number of water molecules per nucleotide) and 84% ($\Gamma \approx 21$). The SE emission from the metal was found to enhance the yields for SSB, DSB and CL by a factor of 3.8 ± 0.5, 2.9 ± 0.7 and 7 ± 3 at $\Gamma \approx 6$, and 6.0 ± 0.8, 7 ± 1 and 3.9 ± 0.9 at $\Gamma \approx 21$, respectively. The study provided a molecular basis for understanding the enhanced biological effects at interfaces in presence of high molecular weight (i.e., high-Z) materials during diagnostic X-ray examinations and radiotherapy.

As the energy of X-rays increases in the experiments of Cai et al., the attenuation in single layered DNA decreases, such that the contribution of SE from the metal to the yield of products becomes concomitantly larger. Taking only the dose imparted by the slow SE emitted from the tantalum substrate, it is therefore instructive to define from the data of Cai et al. [6] a LEE enhancement factor (LEEEF) for monolayer DNA to reflect this energy dependence. The LEEEF is defined as the ratio of the yield of products in monolayer DNA induced by the LEE (slow SE, $E \leq 10$ eV) emitted from the metal substrate *vs* the yield of products induced by the photons in a particular experiment. The LEEEF for 1.5 keV photons was

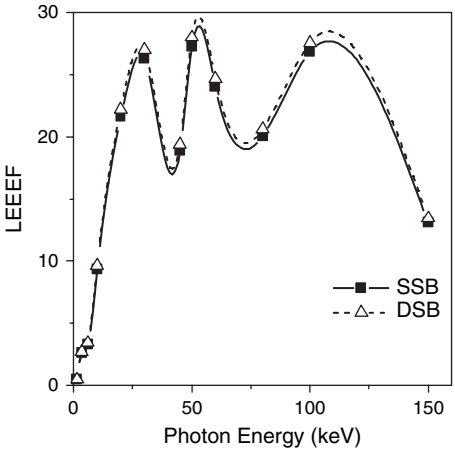

Figure 19-8. Low energy electron enhancement factor (LEEEF) as a function of photon energy for SSB and DSB production in a monolayer of DNA deposited on tantalum

derived to be at least 0.2 for both SSB and DSB. Extrapolation of the LEEEF at higher X-ray energies was made by considering the X-ray absorption coefficient, the total quantum yield of LEEs on photon energy [56] and the spectrum for LEE obtained *vs* photon energy [57]. The extrapolated LEEEF for X-rays from 1.5 keV to 150 keV (i.e., to energies of medical diagnostic X-rays) is shown in Figure 19-8. It indicates that SE emitted from tantalum with an average energy of ~ 5 eV are 20–30 times more efficient to damage DNA in a single layer than the X-ray photons of 40–130 keV. Dividing the values of the LEEEF of Figure 19-8 by the SE coefficient [57], it can be estimated that when LEE strike a single DNA molecule, condensed on tantalum, *they have on average a probability about* 10^5 *larger to damage DNA than* 40–30 *keV photons*. Hence, this first comparison of DNA damage induced by X-rays and SE under identical experimental conditions shows LEE to be much more efficient in causing SSB and DSB than X-rays.

19.5. SELF ASSEMBLED MONOLAYERS (SAM) OF SHORT SINGLE AND DOUBLE DNA STRANDS

19.5.1. Electron Induced Desorption of Neutrals

Due to the bonding selectivity of chemisorption, SAM of DNA can be prepared without significant amounts of impurities. Furthermore, molecular orientation within the layer is fairly well defined [19]. Owing to these characteristics, SAM films of DNA have been particularly useful in the determination of absolute yields and cross sections for specific damages. When extracting attenuation lengths (AL) or cross sections from electron-scattering experiments on thin molecular films, by far the most difficult parameter to determine and control, is the film thickness and its

variation along the plane of the supporting substrate. This problem is particularly acute in the case of vacuum-dried DNA films [18, 31, 42, 52, 58], where clustering of the DNA molecules induces variations in the thickness of the film. These variations translate into errors in the determination of the cross sections for SB by LEE impact [18]. SAM virtually eliminates this major source of error, since in the layer the molecules are uniformly oriented with a regular density over the substrate to which they are chemisorbed [19].

Abdoul-Carime et al. [22, 29] were first to measure the damage produced by LEE impact on SAM of DNA. They measured the yields of neutral fragments induced by 1–30 eV electrons impinging on oligonucleotides made of 6–12 bases. The oligomers were chemisorbed lying flat on a gold surface via the sulfur-bonding technique described in Section 19.2.1. Their results showed that LEE-impact dissociation of DNA led to the desorption of **CN•**, **OCN•**, and/or H_2NCN neutral species from the bases as the most intense observable yields. No sugar moieties were detected; nor were any phosphorus-containing fragments or entire bases. These results were obtained from the MS measurements, explained in Section 19.2.3, of the partial pressure near the target during its bombardment in UHV by a 10^{-8} A electron beam. In Figure 19-9, the black square and the white dots represent the electron-energy dependence of neutral **CN•** and **OCN•** (and/or H_2NCN) yields, respectively. The fragments desorbed per incident electron from oligomers [22, 29] that consist of nine cytosine bases are shown in the upper panel; those desorbed from oligomers consisting of six cytosine and three thymine bases, C_6T_3, are shown in the lower panel. Above 20 eV, the neutral-fragment signals rise with the incident electron

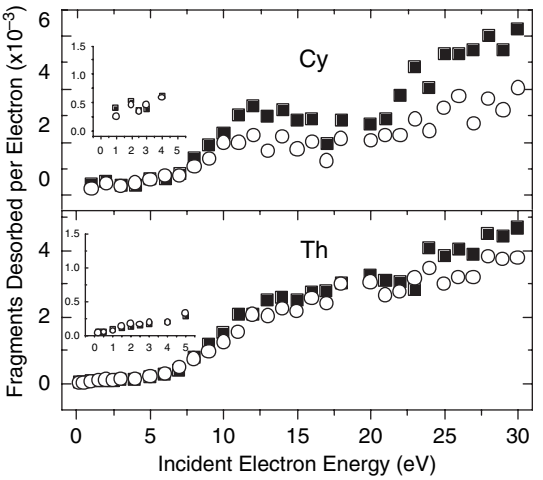

Figure 19-9. Incident-electron energy dependence of neutral CN (*solid square*) and OCN (and/or H_2NCN) (*open circle*) fragment desorption yields per incident electron from C_9 (*upper panel*) and C_6-$(T)_3$ (*bottom panel*) oligonucleotides chemisorbed on a gold substrate. The spread in the data is estimated to be 20%

energy. According to the explanation in Section 19.3, this result is indicative of molecular fragmentation governed mostly by non-resonant DD and/or dissociative ionization of the bases (pathways a → a2 and/or c → c1 shown in Figure 19-3). Below 20 eV, base fragmentation involves resonant and non-resonant excitation to dissociative electronic neutral states (pathways a → a2 and b → b2 → a2 in Figure 19-3) and DEA [20, 22, 29]. Thus, the curves in Figure 19-9 present broad maxima, due to DEA or resonance decay into dissociative electrons excited states, which are superimposed on a smoothly rising signal due to direct electronic excitation. At such relatively high energies (i.e., from 7 to 15 eV for all oligomers), the broad maxima are likely to reflect the formation of core-excited resonances that are dissociative in the Franck-Condon region. This interpretation is supported by: (1) the electron-energy losses in solid-phase DNA bases [59] in the 7–15 eV range, which are attributed to the promotion of π- or σ-orbitals to higher energy ones; (2) the observation of resonant formation of H^- and CN^- at, respectively, 9–10 and 16 eV and 10–15 eV in the ESD yields from thin films of DNA bases [48, 60]. Moreover, the 5 eV threshold of neutral species production coincides with the threshold for electronic excitation.

From the various results of Abdoul-Carime et al. [20–22, 29, 61, 62], it has been possible to determine effective cross-sections or absolute desorption yields per base for base damage induced by LEE impact on homo-oligonucleotides (i.e., oligonucleotides that consist of only one type of base) [22, 29]. As the strand length increased in homo-oligonucleotides from 6 to 9 bases, a decrease in the yield per base was observed; that decrease was attributed to the greater probability of dissociation at the terminal bases [29, 61]. Above nine units, no change larger than 5% of the signal was found. This percentage lies below experimental uncertainties so that the probability of fragmentation of a given base in an oligo can be considered to be constant in strands that contain ≥ 9 bases. Thus, in a nonamer or longer oligo, such measurements provided an absolute determination of the sensitivity of a base to LEE impact. With these absolute yields, it became possible to calculate the expected yields for a specific hetero-oligonucleotide by simply adding the yield for each base contained in the strand. Such projected yields, for ≥ 9-mers oligonucleotides, necessarily assume that the damage is solely dependent on the chemical identity of the base, and does not depend on the environment of the base or sequence. Experimentally, different results were obtained below 15 eV by Abdoul-Carime et al. indicating that the environment of the bases or their sequences play a role in DNA damage induced by LEE [61, 62].

19.5.2. Film Damage Analyzed by Electrophoresis

In a different type of experiment, Cai et al. [63] measured the induction of SB induced by electrons of 8–68 eV in SAM of oligonucleotides. From their results they extracted effective cross sections and AL for SB. A 50-base long thiolated oligonucleotide (OligoS), 5′-$(GCTA)_{12}GC(CH_2)_3$-SS-$(CH_2)_3$-OH-3′ was labelled at the 5′-end with ^{32}P and chemisorbed at 3′-sulfur(S) end onto a gold

substrate. The well oriented OligoS layer [64], having its 5′-end lying at the film-vacuum interface, was exposed to electrons with a constant incident current of 50 ± 2 nA for 3–10 min. Radioactivity measurements of an irradiated portion of the 5′-oligonucleotide fragments (5′-OligoS-F) solution were used to derive the total yield of LEE-induced 5′-OligoS-F, while the rest was concentrated. Fragments from concentrated 5′-OligoS-F were separated by electrophoresis and quantified by phosphor imaging. Molecular weight ladders for identification of the fragments were generated by random depurination. The results obtained from such manipulations, within the linear portion of the exposure response curve, showed that, after subtracting the background from sample manipulation, the yield [(y) in number of fragments] of LEE-induced 5′-OligoS-F decreased with increasing length [(n), number of nucleotide]. The relationship between yield and length for LEE of 8 to 68 eV was well represented by the equation $y(n) = \mathrm{a}e^{-\mathrm{b}n}$, where a and b are constants. Figure 19-10 shows examples of the exponential decrease of the ^{32}P signal as a function of the length of OligoS-F for LEE energies of 8, 28 and 68 eV. A similar dependence was observed for LEE energies of 12, 18, 38, 48 and 58 eV. Above 12 eV, their results showed no significant base preference for SB, suggesting that the mechanism for inducing SB is fairly independent of the nature of the bases or it operates on the sugar-phosphate backbone rather than the DNA bases. This result is consistent with that obtained

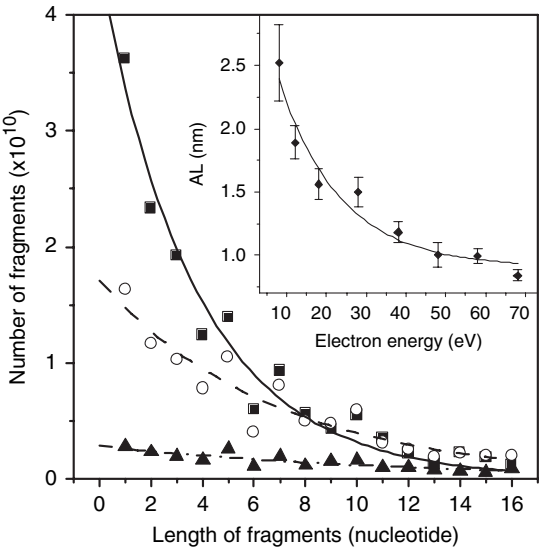

Figure 19-10. Dependence of yield of LEE-induced 5′-oligonucleotide fragments on their length for electron energies of 8 (▲), 28 (◯), and 68 eV (■). The curves represent decaying exponential fits. The inset shows the dependence of the attenuation length (AL) on LEE energy. The error bars represent the uncertainty range of the fitting parameter in the exponential

by Abdoul-Carime et al. above 15 eV, where the yields of CN and OCN from LEE impact on oligonucleotides are not considerably affected by base sequence [61, 62].

Considering that the effective current density for SB decreases exponentially as a function of the electron penetration depth [64], Cai et al. derived the expression for the two fitting parameters as $a = \sigma_{eff}\ N_0\, t\, J_0$ and $b = h/AL$, where σ_{eff} is the average effective cross section for SB per nucleotide, N_0 the initial number of OligoS within the exposure area of the electron beam, t the exposure time, J_0 the incident current density, AL the attenuation length and h the vertical rise per nucleotide [65]. σ_{eff} and AL was thus derived by fitting the yield of OligoS-F versus its length to the equation $y(n) = ae^{-bn}$ for each incident electron energy. The inset of Figure 19-10 shows that AL decrease exponentially with electron energy. The derived AL and cross sections [63] are listed in Table 19-1. The cross section per nucleotide for SB from single stranded DNA at 10 eV has a magnitude of about 9×10^{-18} cm^2, which compares to the value of 1.7×10^{-18} cm^2 obtained at the same energy by Panajotovic et al. [54] in the case of multilayers of physisorbed DNA.

When renormalized to the more accurate cross section at 10 eV obtained by Panajotovic et al., the experimental cross sections for LEE-induced damage to DNA recorded by Boudaiffa et al. [18] give the following values: at 10, 30 and 50 eV, the cross sections per base in a five-layer thick film of plasmid DNA become 1.7×10^{-18}, 1.9×10^{-18} and $2.1\ \times10^{-18}$ cm^2, respectively; i.e. they are at least one order of magnitude lower than those derived by Cai et al. [63] at 8, 28 and 48 eV. The difference lies outside the error limits of both experiments and could therefore indicate that single stranded DNA is more fragile toward LEE impact than double stranded DNA. However, other reasons can be invoked to explain these differences. Since the results of Panajotovic et al. and Boudaïffa et al. were obtained with 5-ML film of DNA, they constitute an effective cross section, but

Table 19-1. Attenuation length and effective cross section for strand breaks (SB) in SAM of oligonucleotides chemisorbed on gold as a function of electron energy

Incident electron energy (eV)	Attenuation length (nm)[a]	Effective cross section for SB ($\times\ 10^{-17}$ cm^2)[b]
8	2.5 ± 0.6	0.3 ± 0.1
12	1.9 ± 0.3	1.7 ± 0.5
18	1.6 ± 0.3	2.8 ± 0.9
28	1.5 ± 0.3	2.0 ± 0.7
38	1.2 ± 0.2	2.6 ± 0.8
48	1.0 ± 0.2	3.2 ± 1.1
58	1.0 ± 0.2	4.4 ± 1.4
68	0.8 ± 0.1	5.1 ± 1.6

[a] The errors represent the sum of the uncertainty range of the fitting parameter b and 10% absolute error in gel quantification; [b] The errors represent the sum of the uncertainty range of the fitting parameter a and 25% absolute error in the measurements.

not an absolute cross section per base. Such an effective cross section contains non-negligible contributions from energy-loss electrons. Furthermore, variation of film thickness and clustering as well as the lower purity in the plasmid experiment should lower the absolute cross sections. The different topology of an oligonucleotide versus a supercoiled plasmid of DNA may also contribute to the differences.

19.5.3. ESD of Anions

As described in the previous section, experiments on LEE induced desorption of H^-, O^- and OH^- from physisorbed DNA films, made it possible to demonstrate that the DEA mechanism is involved in the bond breaking process responsible for SB. The abundant H^- yield was assigned to the dissociation of temporary anions formed by the capture of the incident electron by the deoxyribose and/or the bases, whereas O^- production arose from temporary electron localization on the phosphate group [47]. However, the source of OH^- could not be determined unambiguously, and Pan et al. suggested that reactive scattering of O^- may be involved in the release of OH^- [47]. To resolve this problem, Pan and Sanche [58] investigated ESD of anions from SAM films of DNA. Their measurements allowed both the mechanism and site of OH^- production to be determined.

Their experiments were performed with phosphothioated DNA obtained from substitution by sulfur of the oxygen doubly bonded to phosphorous. The following four different samples were prepared with 40-mers oligonucleotides 5′-GGT ACC AGG CCT ACT ACG ATT TAC GAG TAT AGC GAG CTC G-3′ with and without their complementary strands. A sulphur atom (1S) was substituted at one end of a backbone in the single (ss) and double (ds) stranded configurations (1S-ssDNA and 1S-dsDNA). In other samples, 5 sulphur atoms (5S) were substituted in the backbone in the ss and ds configurations (5S-ssDNA and 5S-dsDNA). Figure 19-11 shows the structure of 1S-ssDNA and the complementary strand in the 1S-dsDNA configuration, with a proton as the counter-ion on the phosphate unit. All samples were chemisorbed by the sulfur atoms on gold substrates. Since the orientation of the DNA molecule with respect to the surface of the substrate depends on the anchoring position, when ssDNA or dsDNA is linked to the substrate at one end (3′ or 5′), the samples have a tendency to stand perpendicular to the gold surface [66]. On the other hand, when the 5S-ssDNA and 5S-dsDNA is anchored on the surface at five different positions along the chain, it lies parallel to the surface [23]. According to the molecular structure in Figure 19-11, the SAM of ssDNA have a terminal sugar with OH at the 3′ position, whereas in the case of dsDNA, one chain is terminated with OH′s at the 3′ and 5′ positions of the sugar and the other has only one terminal sugar with OH at the 3′ position.

The yield functions of OH^- for the four different DNA SAM configurations are shown in curves A–D of Figure 19-12. They all have a threshold at about 2.0 eV, the lowest energy among all anions (i.e., H^-, O^-, OH^-, CH_2^-, CH_3^-, CN^-, OCN^-,

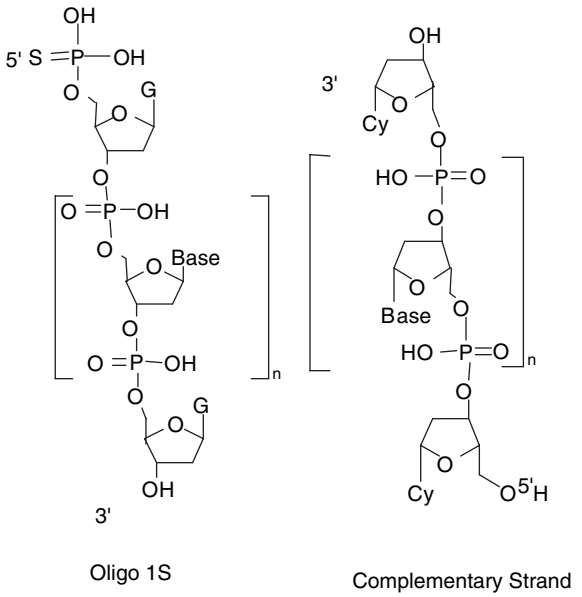

Figure 19-11. The molecular structure of a 40-mer oligonucleotide (1S) and complementary strand. The bracket represents the repeated portion of the strand with different bases (n = 38)

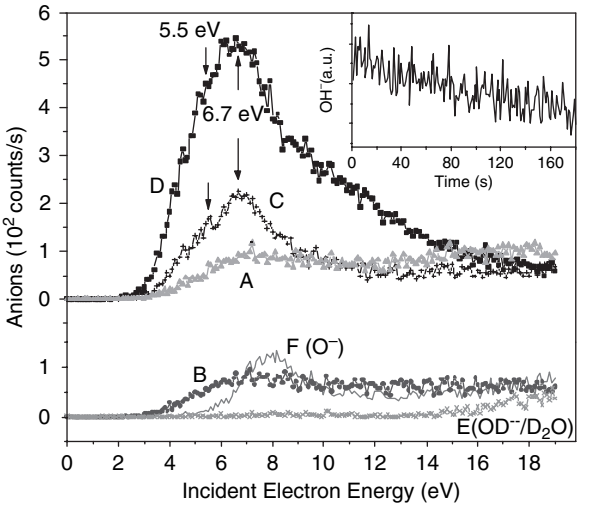

Figure 19-12. Dependence of the OH^- yields on incident electron energy for a SAM of (A) 1S-ssDNA, (B) 1S-dsDNA, (C) 5S-ssDNA, and (D) 5S-dsDNA. (E) represents the yield of desorbed OD^- from a six monolayers water film on Pt and F, the desorbed O^- yield from a 5S-ds DNA film. The inset shows the time dependence of the OH^- signal from a 1S-ssDNA film recorded at an incident electron energy of 7 eV

$OCNH^-$) detected in this type of experiments [67]. The 1S SAM yield functions (curves A and B of Figure 19-12) consist essentially of a broad maximum located around 7 eV, whereas for the 5S SAM (curves C and D) superposition of peaks lying at 5.5 and 6.7 eV followed by very broad structure extending from 8 to 14 eV is observed. The results of Figure 19-12 indicate the formation of OH^- via DEA to DNA; thus OH^- arise from temporary electron localization on a subunit of DNA. In principle, OH^- could also arise from H_2O molecules retained by DNA. However, purposely condensing H_2O molecules on these SAMs considerably diminished the OH^- signal as seen from curve E in Figure 19-12, indicating that OD^- electron-stimulated yields from condensed D_2O films are negligible. The OH^- signal could also arise from DEA to a molecule synthesized by the electron beam during the bombardment. In this case, however, the OH^- signal would increase as a function of time contrary to observation (see inset of Figure 19-12). Reactive scattering [68] could also occur from a reaction between the O^-, produced via DEA to the phosphate group, and the adjacent deoxyribose unit. In this case, the OH^- yield function would bear a resemblance to that for O^- production from which it is derived [68]. However, the O^- yield functions represented by curve F in Figure 19-12 is different from those shown in curves A to D. Since OH is present in DNA only at the terminal sugar and phosphate groups of the backbone, these comparisons leave the possibility of dissociation of a local transient anion at these two positions; i.e., DEA via the reactions

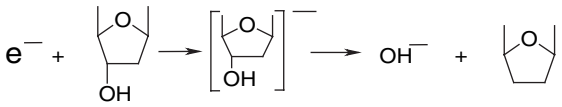

at the 3′ end

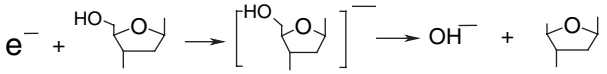

at the 5′ end and

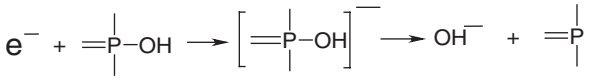

within the backbone.

Considering that the ESD technique is essentially sensitive to constituents near the vacuum-DNA interface, the first two reactions would be favored for DNA standing

perpendicular to the gold surface, whereas the last reaction would be prominent for DNA lying parallel to the surface. The results of Figure 19-12 clearly show that the molecules parallel to the surface give the strongest signal. Thus, the last reaction is favored indicating that below 19 eV electron impact on DNA with OH in the phosphate unit (i.e., the phosphate with H^+ as a counter-ion) produces most of the OH^- via DEA to this unit in the backbone. The phosphate-counterion part of DNA therefore plays a significant role in LEE induced DNA damage.

19.6. THE TETRAMERS GCAT AND CGTA AND OTHER SMALL OLIGONUCLEOTIDES

Much of our present understanding of the mechanisms by which LEE damage DNA derives from experiments with a short strand of the molecule, namely the tetramers GCAT and CGTA. The nomenclature of the tetramer GCAT appears in Figure 19-13, where the potential sites of cleavage yielding non-modified fragments are numbered. These oligonucleotides have been selected for several reasons: (1)

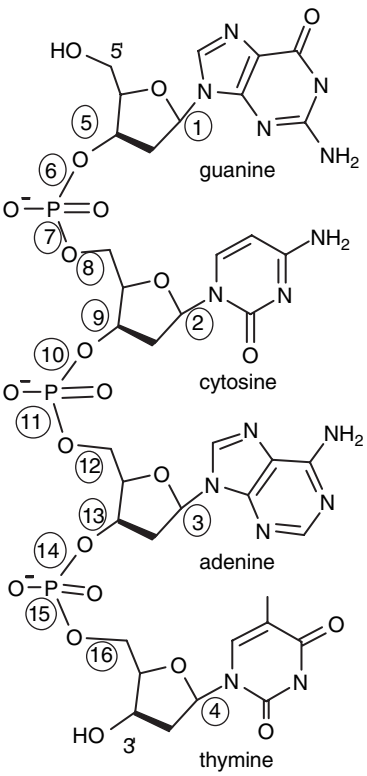

Figure 19-13. Nomenclature of oligonucleotide GCAT with numbered sites of cleavage

they constitute the simplest form of DNA containing the four bases, (2) analysis of degradation products is easier than for longer ss and ds configurations of DNA, (3) comparison with the results obtained with longer strands, allows to study the effect of chain length and (4) comparison with gas-phase data, which is only available for isolated DNA basic components is much easier. The results from ESD of anions from films of these oligonucleotides are reviewed in this section along with those resulting from HPLC analysis of the fragments remaining trapped in the LEE bombarded films.

19.6.1. Analysis of Neutral Fragments

In a series of experiments, Zheng et al. [69–71] analyzed by HPLC the damage induced by LEE to GCAT, CGTA and the abasic forms of GCAT. Such an analysis was made possible by the development of the LEE irradiator, capable of producing large quantities of degradation products, described in Section 19.2. The samples were first irradiated by 10 eV electrons and the analysis focused on the non-modified tetramers CGTA and GCAT along with the formation of fragments, which included monomeric components (nucleobases, nucleosides and mononucleotides), and oligonucleotide fragments (dinucleotides and trinucleotides). The incident electron current and irradiation time were adjusted to give an exposure well within the linear regime of the dose response curve and an equal number of electrons to each sample. The non-modified tetramers were identified in the product mixture by comparison of their chromatographic properties with those of standard compounds.

The reaction of LEE with the tetramers led to the release of all four non-modified nucleobases with a bias for the release of nucleobases from terminal positions. For example, the release of T from the internal positions of CGTA was 3-fold less than from the terminal position of GCAT. The release of unaltered nucleobases from tetramers is likely caused by *N*-glycosidic bond cleavage via DEA from initial electron capture by the base as previously shown in the cleavage of thymidine to thymine in the condensed [72] and gas phase [73]. Table 19-2 gives the amount of non-modified fragments formed in both CGTA and GCAT, based on the HPLC analysis of several bombarded samples. The numbers in the last column correspond to the cleavage positions given in Figure 19-13. In contrast to nucleobases, the release of nucleosides and nucleotides as well as fragments of these occurred exclusively from the terminal positions of each tetramer. The release of monomeric fragments from internal positions requires the cleavage of two phosphodiester bonds. Hence, the lack of these fragments in the product mixture is not too surprising as it simply reflects the result of experiments performed within the linear portion of the dose response curve (i.e. no more than one electron reacts with each target molecule).

For each tetramer, there are eight possible dinucleotide and trinucleotide fragments resulting from 3′ or 5′ cleavage of the four internal phosphodiester bonds. Fragments with a phosphate group were easily detected, but as seen from

Table 19-2. Yield of LEE-induced products of irradiated tetramers. Each fragment is written from 5′ to 3′ with d denoting the deoxyribose unit and p indicating the terminal phosphate group (5′-before or 3′-after the DNA base) with the deoxyribose. The numbers in the last column correspond to the sites of cleavage indicated in Figure 19-13

CGTA (16.8 nmol)		GCAT (16.8 nmol)		
Product	Yield (nmol)	Product	Yield (nmol)	Break position
Nucleobases				
C	0.27 ± 0.05	G	0.22 ± 0.03	1
G	n.d.[a]	C	0.03 ± 0.05	2
T	0.12 ± 0.02	A	0.11 ± 0.01	3
A	0.35 ± 0.07	T	0.35 ± 0.02	4
Nucleosides and Mononucleotides				
Cp	0.29 ± 0.06	Gp	0.11 ± 0.01	8
dC	0.06 ± 0.01	dG	0.00 ± 0.01	6
pA	0.19 ± 0.04	pT	0.23 ± 0.01	13
dA	0.05 ± 0.01	dT	0.10 ± 0.01	15
Dinucleotides and Trinucleotides				
CGp	0.19 ± 0.04	GCp	0.16 ± 0.01	12
CG	n.d.	GC	n.d.	10
pTA	0.11 ± 0.02	pAT	0.22 ± 0.01	9
TA	n.d.	AT	n.d.	11
CGTp	0.20 ± 0.04	GCAp	0.31 ± 0.02	16
CGT	n.d.	GCA	0.04 ± 0.01	14
pGTA	0.23 ± 0.05	pCAT	0.27 ± 0.01	5
GTA	n.d.	CAT	n.d.	7
Total	2.06 ± 0.07		2.15 ± 0.08	

[a] non-detected fragment.

Table 19-2 the corresponding fragments without a terminal phosphate were minor or not detected in the initial product mixture (CG, TA, CGT, and GTA). Finally, the same pattern of cleavage was observed for the loss of mononucleotides from terminal positions of the tetramers. Although this cleavage gave fragments with and without a terminal phosphate, the yield of fragments with a phosphate was much greater than that without a phosphate. So, the formation of 6 major non-modified fragments out of a total of 12 possible fragments for each tetramer indicated that LEE induces the cleavage of phosphodiester bonds to give non-modified fragments with a terminal phosphate rather than a terminal hydroxyl group.

From previous interpretations of SB in DNA, Zheng et al. [69] postulated that rupture of the phosphodiester bond was initiated by the formation of a dissociative transient anion on the phosphate group. The two possible pathways leading to cleavage of the phosphodiester bond are shown in Figure 19-14. Pathway A involves scission of the C-O bond and gives carbon-centered radicals (C5′ or C3′ radicals) and phosphate anions as termini, whereas pathway B results in cleavage of the P-O bond giving alkoxyl anions together with phosphoryl radicals. *Thus, the results of Table 19-2 demonstrate that cleavage of the phosphodiester bond primarily takes*

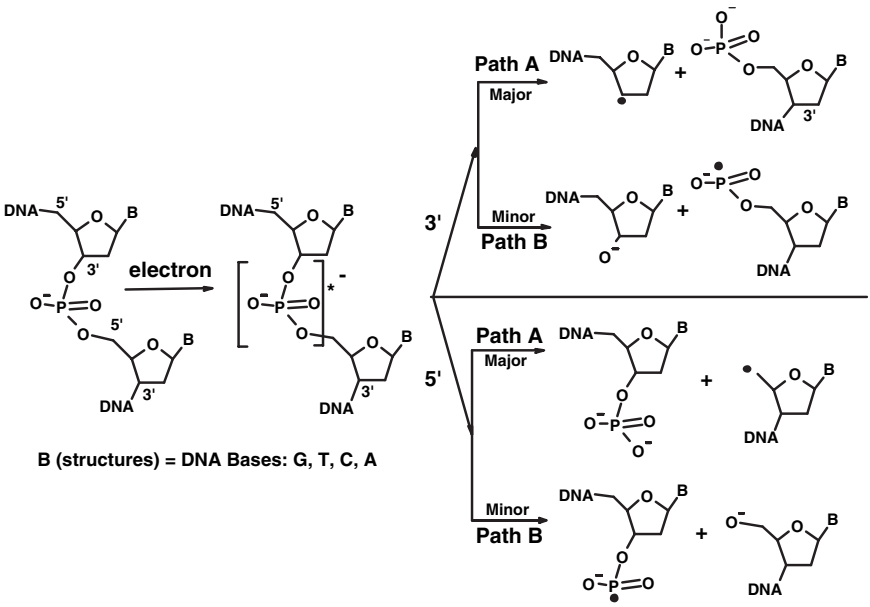

Figure 19-14. Proposed pathways for phosphodiester bond cleavage of DNA via LEE impact

place via C-O *bond cleavage leading to the formation of a sugar radical and a terminal phosphate anion (pathway A)*. The cleavage of C-O and P-O bonds, leading to the formation of phosphoryl radicals and dephosphorylated C3′ radicals of the sugar moiety, was previously reported in ESR studies of argon ion and γ irradiated hydrated DNA [74–76]. The ESR spectra also showed that C-O bond cleavage was the dominant process. In view of the greater bond dissociation energy of the C-O (335 kJ/mol) compared to that of P-O (80 kJ/mol) [77], these data were difficult to explain. A possible interpretation from the results of Zheng et al. [69], is that the bond-breaking process takes place by electron attachment into an unfilled orbital lying at a much higher energy (i.e., 10 eV = 960 kJ/mol) than the thermodynamic threshold of C-O bond dissociation. In this case, phosphodiester bond cleavage would not depend on bond energy considerations, but rather on the availability of dissociating anionic states at the energy of the captured electron.

In subsequent investigations, Zheng et al. measured the yields of the products listed in Table 19-2 as a function of electron energy for GCAT [70]. From 4 to 15 eV, scission of the backbone gave non-modified fragments containing a terminal phosphate, with negligible amounts of fragments without the phosphate group. This indicated that phosphodiester bond cleavage involves cleavage of the C-O bond rather than the P-O bond within the entire 4–15 eV range. Most yield functions exhibited maxima at 6 and 10–12 eV, which were interpreted as due to the formation of transient anions leading to fragmentation. Below 15 eV, these resonances dominated bond dissociation processes. All four non-modified bases

were released from the tetramer within the 4–15 eV range, by cleavage of the *N*-glycosidic bond, which occurred principally via the formation of core-excited resonances located around 6 and 10 eV. The incident electron energy dependence of the yield of the bases is shown as an example in Figure 19-15.

With the exception of cytosine, whose maximum occurs at 12 eV, the other curves exhibit maxima at 10±1 eV. Such 10–12 eV peaks were always present in the yield functions of all other products, whereas the 6 eV peak appeared in the yield functions of the monomers dG and dGp and oligomers pCAT and pAT. The strongest monomer signal, which exhibited a maximum at 10±1 eV, was found in the yield function thymidine phosphate (pT). Interestingly, with the exception of the very small yield for the production of dG and cytosine, a strong dip in all yield function was present at 14 eV, partly because of the sharp rise in the yield beyond that energy. As seen from comparison with Figures 19-5 and 19-6, this strong minimum has been observed in the yield functions for SSB and DSB in films of dry plasmid DNA [31] as well as in the yield function for H^- , O^- and OH^- desorption induced by LEE on similar films [47]. Moreover, there exists a striking resemblance between the yield functions obtained from GCAT and that for SSB from plasmid DNA, as seen from comparison of Figure 19-5 with Figure 19-15; i.e., a dip near 14 eV, a shoulder near 6 eV and a broad peak around 10 eV.

The broad peaks at 6 and 10 eV, which are present in the yield functions for various types of DNA damage, are likely to be due to the formation of core-excited or core-excited shape resonances, since the lifetime of such resonances is usually sufficiently long to promote dissociation of the anion. A priori, scission of the C-O bond leading to SB can occur by direct electron capture on the phosphate group

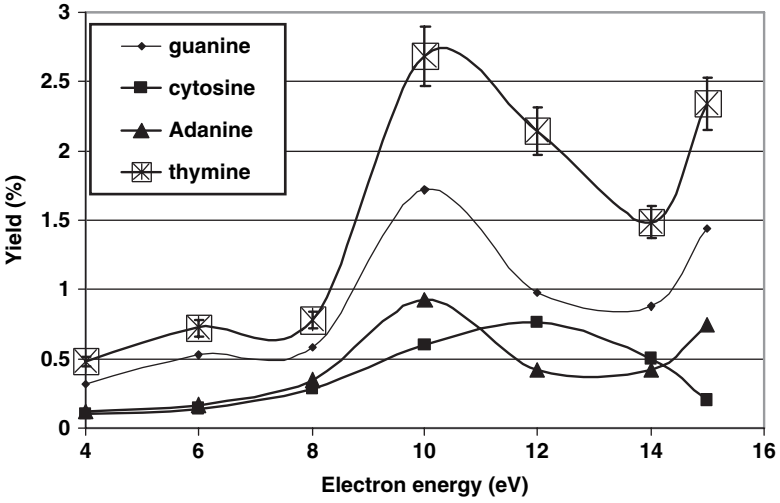

Figure 19-15. Dependence of the yield of nucleobases on the energy of 4–15 eV electrons. The error bars represent the standard deviation (9%) of eight individual measurements fitted to a Gaussian function

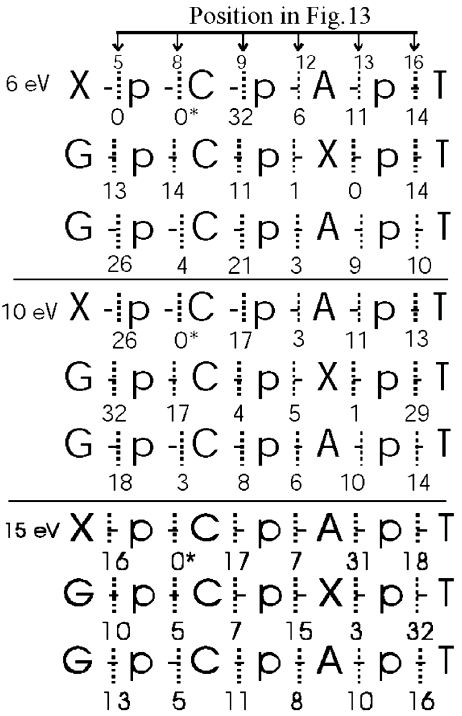

Figure 19-16. Percentage distributions of strand breaks by sites of cleavage, induced by 6, 10, and 15 eV electrons. *Xp was not detected by HPLC and the yield was considered to lie below the detection limit

or via electron transfer from a base to the phosphate moiety. However, transfer of a core-excited or core-excited shape resonant state to other basic unit is unlikely because it requires a three-electron jump [78]. Hence, it has been conjectured that such resonances are responsible for ESD of H^- from the bases of DNA (Figure 19-6). For shape resonances, the lifetime is usually too short above ~5 eV for dissociation [34, 79] and electron detachment or transfer is highly probable due

Table 19-3. Comparison of damage yield of tetramer at electron energies of 6, 10 and 15 eV (standard deviation = 10%)

Yield (%)	6 eV			10 eV			15 eV		
	Strand break	Base release	Total	Strand break	Base release	Total	Strand break	Base release	Total
XCAT	0.72	0.39	1.11	1.11	0.45	1.56	9.89	1.14	11.03
GCXT	0.80	0.60	1.40	4.56	0.56	5.12	2.34	0.78	3.12
GCAT	4.76	1.96	6.72	9.54	5.92	15.46	10.30	4.72	15.02

to the considerable overlap between the wave functions for an additional electron on each basic DNA unit. Since above 14 eV electron resonances are not expected to dominate the electron scattering process, the yields in Figure 19-15 should represent mostly dissociation via direct excitation of dissociative electronically excited states.

In order to provide additional information on the hypothesis of electron transfer from a base to the phosphate group of DNA, Zheng et al. [71] analyzed the products induced by 4–15 eV electrons incident on two abasic forms of the tetramer GCAT, i.e., XCAT and GCXT, where X represents the base replaced by a hydrogen atom. With the exception of the missing base, the same fragments were observed in the mixture of products from irradiated GCAT tetramers with [71] or without [70] an abasic site. Table 19-3 provides a comparison of the yields expressed as the percentage of SB and base release from the initial amount of tetramer before bombardment at 6, 10 and 15 eV. Yield functions for GCXT were also produced from such yields for all fragments recorded at seven different energies between 4 and 15 eV. The yield of each fragment resulting from SB as a percentage of the total damage to a particular tetramer is shown in Figure 19-16, where the percentage of fragments corresponding to bond cleavage at different positions along the chain, is given for bombardment of XCAT, GCXT and GCAT at 6, 10 and 15 eV. It is obvious that at 6 eV, when G is absent (i.e., in XCAT), there is no cleavage of the phosphodiester bond at the position lacking the base moiety. Similarly, when A is removed (i.e., in GCXT), there is practically no dissociation of the C-O bonds on either side of A. *Thus, at* 6 *eV, G and A must be present within GCAT to produce C-O bond rupture next to the base (positions* 5, 12 *and* 13 *in Figure 19-13).* It is difficult to explain this result without invoking electron capture by G and A followed by electron transfer to the corresponding phosphate group. This phenomenon is not observed at 10 and 15 eV, with the exception of bond rupture at position 13, which decreases from 10% in GCAT to 1% in GCXT at 10 eV.

Since electron transfer from a DNA base π^* to a C-O σ^* orbital had been shown theoretically to occur at energies below 3 eV [80], Zheng et al. [71] suggested that the incident 6 eV electron electronically excites a base before transferring to the C-O orbital. They based their suggestion on the existence of electronically excited states of the DNA bases within the 3.5 to 6 eV range measured by electron-energy-loss spectroscopy [59, 81]. For example, LEE energy-loss spectra of thymine exhibit electronically excited states at 3.7, 4.0 and 4.9 eV ascribed to excitation of the triplet $1^3A'$ ($\pi \rightarrow \pi^*$), $1\ ^3A''$ ($n \rightarrow \pi^*$) and ($\pi \rightarrow \pi^*$) transitions [81]. Excitation of these states by 6 eV electrons forming a core-excited shape resonance on T would produce electrons of energies below 3 eV, which could then transfer to the phosphate-sugar backbone. In other words, the 6 eV resonance would decay by leaving one hole and one electron in a previously empty orbital on the base and the excess electron would be coupled to an empty σ^* CO orbital on the backbone via through-bond interaction. This hypothesis implies a strong decay of core-excited resonances into electronically inelastic channels, a phenomenon which has recently been demonstrated theoretically by Winstead and McKoy [82]. Zheng et al. [71] denoted this decay channel as the "electron transfer channel". Energy-loss electrons

could also transfer into π^* orbitals of adjacent bases, which lie in the range of 0.29–4.5 eV [53], before transferring to the backbone. Thus, by resonance decay to the electron transfer channel following excitation of the bases, electrons having the energies in the range for transfer [79] would be created and lead to C-O bond scission. If the transient anion and/or the final electronically excited state on the DNA base are dissociative, it could lead to scission of the N-glycosidic bond, thus causing base release or simply leave DNA with a modified base. Alternatively, the transferring electron could temporarily localize at or near the N-glycosidic bond and form a shape resonance at a lower energy, which could be dissociative. In fact, the results in Table 19-3 may be representative of coupling of such electrons between the bases followed by scission of the N-glycosidic bond. They also reinforce the hypothesis of electron transfer to the phosphate group.

It is seen from Table 19-3 that removing a base in GCAT causes a drastic reduction in the quantity of damage at 6 and 10 eV. For example, at 6 eV, SB are reduced by a factor of about 6 and base release by a factor of 3.3 and 5 for GCXT and XCAT, respectively. In a classical picture, where the damage caused by electron capture by DNA bases is simply additive and rupture of all the N-glycosidic and C-O phosphodiester bonds are given the same probability, we would expect that the amount of SB and base release in the abasic tetramers to decrease by ~25% (i.e., to be 3.57% and 1.47%, respectively). This nonlinear decrease in damage caused by introduction of an abasic site is also reflected in the yield functions from GCXT for all fragments recorded by Zheng et al. [71]. This suggests that the magnitude of damage in GCAT is caused by a collective effect involving DNA bases, which appears to be strongly suppressed by removal of G or A. In other words, electron-molecule scattering within DNA must be highly sensitive to the number of bases and the overall topology of GCAT. Although we have no information on the topology of these tetramers, recent calculations of LEE scattering from and within DNA show that the ordering of DNA bases, in a helical configuration within the molecule, strongly influences the electron capture probability by these components [83]. More specifically, the electron capture probability by DNA bases for partial waves of certain momentum has been found to increase up to one order of magnitude, owing to constructive interference of these partial waves within DNA. Since these interferences are related to the presence and relative position of the bases and oligomer topology, they should be considerably modified when the stacking arrangement is changed by base removal. The differences in the yields from GCXT (or XGAT) and GCAT could, in fact, result not only from the different nature of the base removed, but also from the different geometrical configurations of the molecules. For example, at 15 eV, according to this diffraction mechanism [82] and the results in Table 19-3, the structure of XCAT would not be much influenced by interference in the internally scattered electron wave thereby giving the expected decrease of about 25% less damage than in GCAT; but, constructive interference would vanish in GCXT, where the yield drops by a factor of about 5 compared to that from GCAT.

The introduction of an abasic site in the tetramer also considerably reduces interbase electron transfer, particularly in GCXT, where electron capture by T and C from a transient anion on A would be inhibited. However, even if we assume that all electrons captured by G are transferred to C, the yield of SB and base release would be reduced only by a factor of 2 in XCAT, which is insufficient to explain the data of Table 19-3 at 6 and 10 eV. Although, inhibition of interbase electron transfer could play an important role in the nonlinear decrease of damage due to base removal; electron diffraction must still be invoked to explain the magnitude of this decrease. Finally, the results of Zheng et al. do not eliminate the possibility that some of the SB occur without electron transfer (i.e., from direct DEA to the phosphate group), but with a much reduced intensity. In fact, DEA in thin films of the phosphate group analog NaH_2PO_4 leads to rupture of O-H bonds, within the 4–10 eV range [84]. The same bonds within the DNA backbone correspond to those linking oxygen with carbon atoms.

The decomposition of longer oligonucleotides with the sequences $G_6T_3G_6$ and dT_{25} by ~1 eV electrons was studied by Solomun et al [85, 86]. The single stranded oligonucleotides were immobilized on a gold surface in a micro array format. After electron irradiation, the decomposition of the oligonucleotides was measured by fluorescence. In the case of dT_{25}, Solomun et al. [85, 86] estimated (assuming 10^{13} oligonucleotides/cm^2) a value for the total damage cross-section of about 1.5×10^{-16} cm^2. The latter value compares to the cross section of 5×10^{-17} cm^2 at electron energy of 12 eV obtained by Dugal et al. [20] in measurements of neutral fragment desorption from SAM of single stranded 12-mer oligonucleotides. This value can also be compared with that of 1.7×10^{-17} cm^2 at 12 eV per nucleotide from the experiment of Cai et al. [63] for SSB in ss oligonucleotides. The results of Solomun et al. [85, 86] implied that ssDNA and ssRNA are much more endangered during replication, transcription or even translation stages than the current radiation damage models envisaged.

Collisions between 1 and 100 eV electrons and negatively charged oligonucleotides consisting of 2 to 14 bases were studied using an electrostatic storage ring with a merging electron-beam technique by Tanabe et al. [87]. The rate of neutral particles emitted in the collisions was measured as a function of 1–4 negative charges and number of bases in the oligonucleotide. The rate started to increase from definite threshold energies. These energies increased regularly with ion charges in steps of about 10 eV starting at about 10 eV for a single electron charge. They were almost independent of the length and sequence of DNA. The neutral particles came from breaks of DNA, rather than electron detachment [87]. The 10-eV step of the increasing threshold energy approximately agreed with the plasmon excitation energy [88]. From these experiments, Tanabe et al. deduced that plasmon excitation is closely related to the reaction mechanism [87].

19.6.2. ESD of Anions

ESD of anions from thin films of GCAT and its four abasic forms has been investigated by Ptasiñska and Sanche [89, 90]. For all these forms, the H^- , O^- and

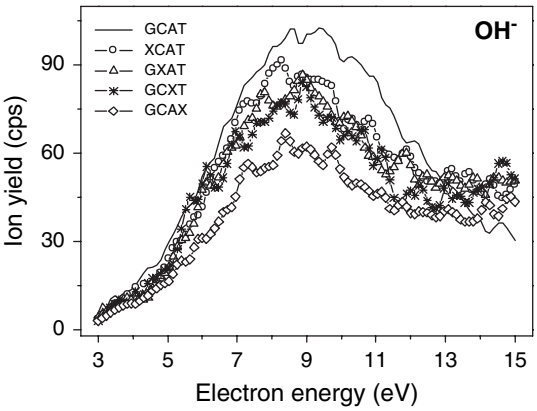

Figure 19-17. LEE stimulated desorption yield of OH^- from the GCAT tetramer and its abasic forms

OH^- yield functions between 6 and 12 eV impact energies exhibited resonant peaks indicative of DEA to the molecules. Above 14 eV, nonresonant DD dominated the ESD yields. The yield function for OH^- from GCAT [89] and its abasic forms [90] is shown in Figure 19-17. Similar curves were obtained for the H^- and OH^- yields, but the relative magnitude between GCAT and its abasic forms was different [72]. These differences are illustrated by the numbers in Table 19-4, which provide the energy integrated intensities between 3 and 15 eV along with the relative yield of H^- , O^- and OH^- from each abasic tetramer considering the yield from GCAT to be 100%.

In their studies, Ptasiñska and Sanche [89] compared the anion yield functions obtained from GCAT to those recorded for corresponding anions from isolated subunits of DNA, i.e., the nucleobases and sugars in the gas phase and the phosphate group in the condensed phase [84, 91–103]. The DEA processes found in the gas phase were still present within GCAT, but some transient anions were suppressed, particularly at low energies, because of the existence of chemical and/or hydrogen bonds within DNA or the insufficient kinetic energy of the stable anions formed. Additionally, the surrounding medium was found to favor specific dissociation processes, e.g., the formation of OH^- , which had not been observed in gas-phase studies. An example of comparison with gas-phase data from isolated bases is shown in Figure 19-18. This figure shows the CNO^- yield obtained from summing the signal from all bases in the gas phase [92, 93] along with that observed for GCAT films. The CNO^- anion was observed only for pyrimidines, C and T [93]. The lower energy peaks seen in the gas-phase experiments are not observed in the case of the tetramer. Thus, it appears that CNO^- formations are inhibited by sugar bonding at the N1 position in DNA; however, low kinetic energies of the CNO^- fragments could also prevent desorption from the surface.

In contrast to the yield of SB and base release, the magnitude of anion desorption does not depend very much on the presence of an abasic site in GCAT [90], as seen

Table 19-4. Measured H^- , O^- and OH^- LEE induced desorption signals (in arbitrary units) from thin films of the tetramer GCAT and its abasic forms. The percentage of the signal for each anion is given in the last column taking the yield from GCAT to be 100%

	form	area (a.u)	%
H^-	GCAT	702223.0	100
	XCAT	586589.6	83.5
	GXAT	591955.6	84.3
	GCXT	694797.8	99.0
	GCAX	621214.1	88.5
O^-	GCAT	752.2	100
	XCAT	545.9	72.6
	GXAT	581.0	77.2
	GCXT	667.4	88.7
	GCAX	519.4	69.1
OH^-	GCAT	716.4	100
	XCAT	643.8	89.9
	GXAT	613.1	85.6
	GCXT	589.2	82.3
	GCAX	466.9	65.2

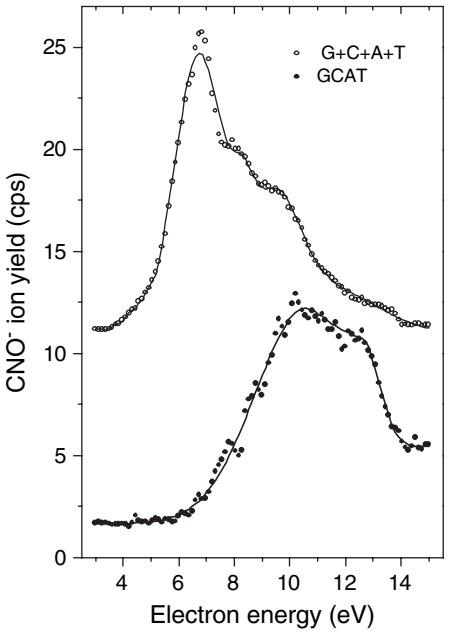

Figure 19-18. CNO^- ion yield function from a film of GCAT and the summation of ion yields for corresponding anions observed from nucleobases in the gas phase (G + C + A + T)

from Table 19-4. From a purely classical point of view, if the anion signals arose exclusively from initial electron attachment on a base and if each base were given an equal weight for producing these anion yields, we should observe the anion signals from the abasic tetramers to be 75% of that from GCAT. For H^- the signal averaged for all abasic tetramers is higher (88%) than this value, whereas for O^- it averages close to 75%; for OH^- the averaged signal diminished to 81%. These results clearly indicate *the absence* of quantum interference or coherent effects in the interaction of the incident electron with DNA leading to DEA (i.e., the OH^- and O^- yields are merely proportional to the number of bases). In fact, according to theory, coherent enhancement of the wavefunction of the electron initially scattered within DNA is relatively modest at 9–10 eV, but below 4 eV can reach one order of magnitude for $\ell = 2$ partial waves and two orders of magnitude for $\ell = 3$ partial waves [83, 104, 105]. In general, as the electron energy decreases, its de Broglie wavelength increases and the electron becomes more delocalized and hence diffraction, which is structure dependent, becomes prominent. The yields being on average remarkably higher than 75% for H^- , the additional contribution possibly arises from the sugar group, which is not expected to be considerably affected by the creation of an abasic site. In fact, in the results of experiments with 40-base pair and plasmid DNA, shown in Figure 19-6, the H^- signal is observed to arise from both the bases and the sugar group [47].

These same experiments, as well as those performed with SAM of ss and dsDNA [58] also demonstrate that both the O^- and OH^- (see Figure 19-12) signals arise from DEA to the phosphate group. If such DEA processes arose only from direct attachment to the phosphate group, no significant decrease would be observed in the O^- and OH^- signals from the abasic tetramers, unless the resonance parameters on the phosphate transient anion corresponding to the position of the missing base are modified, so as to essentially suppress all anion desorption from that position. Since the latter hypothesis is unlikely, the results of Figure 19-12 and Table 19-4 suggest that *electron transfer from the bases to the phosphate group occurs in the formation of* O^- *and* OH^- *via DEA of* 5–12 *eV electrons to DNA, but without diffraction effects.* Whereas O^- almost exclusively arises from the double bonded oxygen of the phosphate group in long DNA chains, in the case of a small oligonucleotide like GCAT, contributions to the OH^- signal can also arise from the OH group of the terminal bases.

Anion ESD yields from GCAT were also recorded under hydrated conditions [91]. Three ML of water were deposited on GCAT films; this amount corresponds, on average, to 5.25 H_2O molecules per nucleotide at the surface of an oligomer film. It does not include the 2.5 structural H_2O molecules per nucleotide, which cannot be removed from DNA under vacuum conditions [106]. Assuming a uniform water distribution, such two-component films represent DNA with the addition of 60% of the first hydration shell.

Figure 19-19(a) presents H^- ion yields obtained from a pure film of GCAT, a 3 ML thin film of H_2O and a two-component target consisting water and GCAT. The yield function of H^- observed from a H_2O/GCAT film displays two prominent

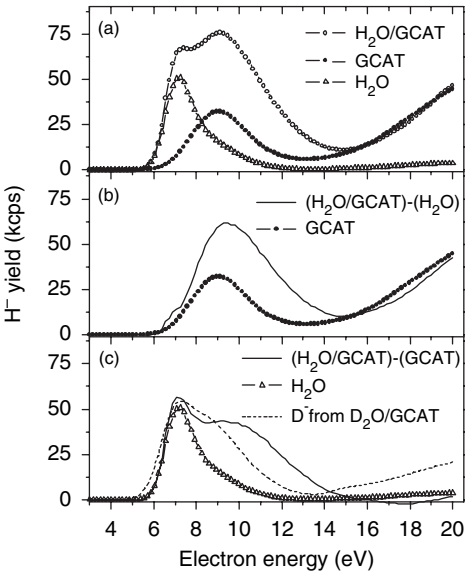

Figure 19-19. (a) The H^- ion yield functions obtained from GCAT (*solid circle*), 3 ML of water (*open triangle*) and two-component films: H_2O/GCAT (*open circle*). (b) The H^- ion yield function from a H_2O/GCAT film from which the ion yield of H^- recorded for H_2O is subtracted. (c) The H^- ion yield function from a H_2O/GCAT film from which the ion yield of H^- recorded for GCAT is subtracted. The D^- yield from D_2O coverage of GCAT is shown in (c) by the *dash line*

peaks that are separated from one other by about 2 eV. The largest peak at 9.3 eV appears to be associated with the signal arising from pure GCAT, which also exhibits a peak at 9.3 eV. The first feature peaking at 7.3 eV can be associated to DEA via resonant capture of the electron in the $^2B_1$ state of H_2O. Such feature is characteristic of H_2O molecules embedded in an amorphous water ice environment [107] and suggests that some regions of the DNA, absorb more water molecules than others.

Figure 19-19(b) and (c) present the anion yield functions obtained by subtraction of the H^- desorption signal observed for pure H_2O and GCAT films from the H_2O/GCAT curve in Figure 19-19(a). The yield functions of GCAT and H_2O are also shown in Figures 19-19(b) and (c), for comparison. Subtraction of the H_2O signal from that of the mixture film should have led to the yield function of GCAT, if the resulting signal arose from a linear combination of desorption yields of both components. This is not the case; the resulting difference yield function has a larger magnitude and extends to higher energies, indicating that it arises completely or partly from another type of dissociative transient anion. The latter can be seen as a perturbation of the original anion formed with a base GCAT or with H_2O, by the interaction of H_2O with the oligomers; it can also be seen as a new type of anion whose parent is a complex resulting from the interaction of H_2O with DNA (i.e., a GCAT-H_2O complex). Similarly, subtracting the GCAT signal from that of the mixture film does not entirely reproduce the H_2O yield function and

results in a difference yield function having an additional broad peak around 10 eV. This peak represents the signal arising from the GCAT-H_2O complex, since any contribution from intact GCAT has necessarily been subtracted. This new core-excited resonance, lying in the 9–10 eV region, is different in magnitude and width from the 9.3 eV resonance in pure GCAT. It corroborates previous infrared laser spectroscopy studies, ab initio calculations [108] and calorimetry measurements [109], which have demonstrated the existence of a strongly bonded DNA-H_2O complex. The formation of this complex not only influences H^- desorption from the bases of GCAT, but it was also found [91] to modify H^- desorption from the water molecule. The presence of this complex can also be seen in the O^- and OH^- yield functions, from which it has been shown that O^- emanates from the counter ion on the phosphate group of GCAT [91]; i.e., where the water molecule binds preferentially.

19.7. SUMMARY AND CONCLUSIONS

Our present comprehension of LEE-induced damage to DNA has evolved from both experiments and theoretical models. These latter have either not incorporated the complete molecular nomenclature of the basic units of the molecule or have been limited to short single strands composed of only few basic units and electron energies below about 3 eV. Many of these models have shown that electron capture by short DNA segments could lead to SB. Depending on basic units in the model, however, different mechanisms have been found to dominate bond scission within the backbone or elsewhere in DNA. For example, Simon's group [11–13], examined a range of electron kinetic energies representative of the energy width of the lowest π^*-resonance states of the bases and determined how the rates of cleavage of the sugar-phosphate C-O σ bond depend on energy and on the solvation environment. In their studies, they showed that electrons of ca. 1.0 eV could attach to form a π^* anion on a base, which then could break either a 3′ or 5′ O-C σ bond connecting the phosphate to either of two sugar groups. For both cytosine and thymine, Simons and co-workers [11–13] evaluated the adiabatic through-bond electron transfer rate with which the attached electron moves from the base, through the deoxyribose, and onto the phosphate unit and then causes cleavage of the sugar-phosphate σ bond. Their calculations show that the SSB rate due to electron transfer depends significantly upon the electron energy and the solvation environment near the DNA base. Later Gu et al. [110] showed that electron transfer from the π^* orbital of the pyrimidine anion to the DNA backbone does not pass through the N1-glycosidic bond. Instead, it occurs through atomic orbital overlap between the C_6 of pyrimidine and the C_3' of the ribose. In a sugar-phosphate model, Li et al. [111] also studied theoretically cleavage of this bond by an electron weakly bonded to the sugar-phosphate group. They found that above ~0.5 eV direct electron attachment to the phosphate group without electron transfer from the bases leads to stretching the C-O^- bond, thus causing the initial transient anion state to cross over to the σ^* orbital. This change of orbital symmetry leads to 3′ and 5′ O-C bond cleavage, if the lifetime of the

σ anti-bonding state is sufficiently long. According to the work of Berdys et al. [12, 13] near 0 eV electrons may not easily attach directly (i.e., vertically) to the phosphate units, but can produce the metastable P = O π^* anion above 2 eV.

There exists also the possibility of proton transfer to the negatively charged base during the lifetime of a resonance. Such a transfer would leave an extra electron on the sugar or phosphate unit, which could also lead to rupture of the sugar-phosphate CO bond. This mechanism has been investigated with DFT calculations for proton transfer to cytosine at thermal energies [112]. Proton transfer is impossible for the neutral nucleoside, but proceeds to a barrier-free C-O cleavage for negatively charged cytosine. It has also been found from recent calculations on electron scattering from a simplified model of A and B forms of DNA that owing to internal electron diffraction within DNA strands, the capture probability is much larger on the phosphate group than on any of the other basic units [104]. Finally, by incorporating two phosphate groups in their model, Gu et al. [15] showed that the excess electron locates both on a base and on the phosphate moiety in single DNA strands.

As shown in this review article, the LEE-damage mechanisms deduced from experiments are not limited to the very low energy range (E<3 eV) as in the case of theoretical calculations with short DNA strands. Similar to theoretical modeling, however, taken separately these experiments do not always allow unambiguous identification of the prominent mechanism leading to specific damages at a given energy. For example, the results of Figure 19-16 obtained at incident energy of 6 eV showed that essentially no strand break occurs at positions in the backbone corresponding to those of the missing base. *This finding may be seen as a clear indication that at 6 eV, and possibly below, electrons break the DNA backbone almost exclusively via electron transfer, whereas at higher energy direct electron attachment to the phosphate group contributes to SB.* However, it could be argued that C-O bond scission in the backbone occurs only via direct DEA to the phosphate group, but base removal affects the resonance parameters of the transient phosphate anion, so as to diminish considerably C-O bond dissociation (e.g., reduce the lifetime of the transient anion state). Taken separately these two hypotheses appear plausible, but the latter restrains the primary electron interaction to the backbone, which is contrary to many calculations and the measured magnitude of base release and SB. The yields of products corresponding to these breaks strongly decrease with abasic site formation, as explained in Section 19.6. Such a behavior requires the electron interaction to involve a number of bases. Without invoking electron diffraction between the bases, which amplifies localization on the bases and thus electron transfer to the phosphate group and $N-$glycosidic bond, it is not possible to explain the overall decrease in base release and SB shown in Table 19-3, upon abasic site formation. In other words, it is difficult to imagine how a missing base could modify the resonance parameters at all sites of the tetramer, so as to cause, for example, an order of magnitude decrease of the damage at 10 eV.

More generally, by considering the results reviewed in the present article and various theoretical calculations, it appears possible to provide a unique model of

0–15 eV electron interaction of LEE with DNA consistent with all observations and calculations. First, the incoming electron can interact simultaneously with a multiple number of successive basic DNA units (i.e., along the bases or the backbone). Depending on electron energy, topology of the DNA and surrounding medium it results constructive or destructive interference of the electron wavefunction. Such diffraction is more pronounced at very low energies ($E_0 < 3$eV), where the electron wavelength compares to the inter-unit distances within DNA (3–4 nm).

As diffraction takes place an incident electron of energy $E_0 < 15$ eV can localize on a subunit (SU) and form a local transient anion of that unit as shown on top of Figure 19-20. The transient anion $[SU]^-$ can be a shape, a core–excited or a core-excited resonance. At energies below the first electronically excited states of DNA, only shape resonance can be produced and it is in this energy range that shape resonances possess a sufficiently long lifetime to cause dissociation of molecular bonds via DEA. *In fact, since no neutral electronic states exist at such energies the only mechanism capable of breaking bonds is DEA.* Hence, as shown in Figure 19-20, the electron can leave the SU unaltered with its initial energy E_o (pathway 1) or DEA can occur (pathway 2). In the case of pathway 1, the electron can be released into the continuum (e_c^-) (i.e., the surrounding medium or vacuum) or it can be transferred (e_c^-) elsewhere within DNA. So far, most calculations show that both pathways (1 and 2) lead to SB for shape resonances below 3 eV, with a preference for electron transfer. In one case, the electron is captured by a base and transferred (e_t) to the phosphate moiety causing rupture of the C-O bond; in the other, direct DEA to the phosphate group causes the break. At the experimental level, the results of Figure 19-7 show that the preferred mechanism for SB is

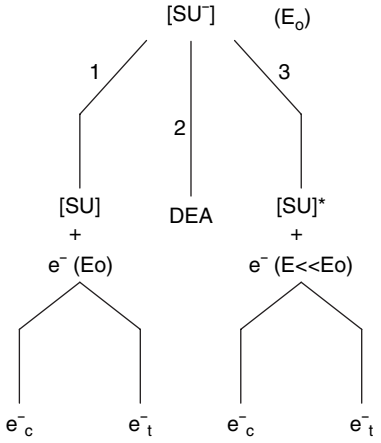

Figure 19-20. Decay channels of a transient anion of a fundamental DNA unit (SU) formed at electron energy E_0. Pathway 1, 2 and 3 represent the elastic, DEA and electronically inelastic channels, respectively. In channels 1 and 3, the additional electron can be emitted in a continuum of states (e_c^-) or transferred to other DNA subunits (e_t^-)

electron transfer from the bases with a possible background contribution from direct DEA to the phosphate moiety.

At energies close to and above that required to produce the first electronically excited state, shape and core-excited $[SU]^-$ resonances can be formed. The latter are well localized in DNA, since their motion within the molecule requires a 3-electron jump. In the energy range of core-excited resonances, the only decay channel of shape resonances is pathway 1 as they are considered to be too short-lived to cause dissociation. *Thus, at those higher energies, core-excited resonances are usually considered to be responsible for DEA*. Such transient anions have therefore been considered responsible for the resonance features observed in anion ESD from DNA, including production of O^- via the temporary localization of 8.2 eV electrons on the π^* double bond of the phosphate group [84], OH^- desorption by the localization of 4.3 and 6.3 eV electrons on the protonated form of the phosphate group [58] and desorption of H^- as the result of temporary capture of 8–12 eV electrons on the bases with a small contribution from a core-excited resonance on the sugar group [47]. Base release was ascribed to core-excited resonance decay into dissociative electronic excitation and/or DEA channels of the detaching base [69, 70] (i.e., pathway 3 and/or 2, respectively). The pathway 3 channel occurs when the energy of a core-excited resonance lies above the first electronically excited state of the parent neutral SU. In general, decay by electron emission can leave the SU in the ground state (pathway 1) or in an electronically excited state, which can be dissociative or not. Thus, another pathway (3 in Figure 19-3) becomes accessible for electron emission. In this case, the departing electron has energies $E << E_0$. Furthermore, the energy-loss electron can be emitted into the continuum (e_c^-) or stay within DNA (e_c^-). Hence, electron transfer in the energy range of core-excited resonances can occur via different routes (1 and 3).

Via pathway 1, the extra electron can be reemitted within DNA without losing significant amounts of energy. Consequently, this delocalized electron can relocalize on the phosphate group, where again it can form a shape or core-excited resonance. In the case of pathway 3, the extra electron on the base undergoes the same transfer process, but with lower energy, leaving the base in an electronically excited state. To produce SB, pathway 1 requires a final core-excited anion state to exist near 9–10 eV on the phosphate group, be dissociative and live a sufficient time for the C-O bond to break. Core-excited resonances exist within the range 5–12 eV and were found to lead to H^-, O^- and OH^- production from NaH_2PO_4 [84]. However, this pathway cannot explain the strong collective effect observed in the SB yield data of Zheng et al. [71]. Furthermore, if both SB and DEA to the phosphate group occurred via pathway 1, they should exhibit the same diffraction effects; as seen from Figure 19-19, no diffraction effects are present in the ESD yield of anions. *Thus, pathway* 3 *is to be preferred as a mechanism to explain most of C-O bond scission in the DNA backbone, whereas pathway* 1 *and* 2 *could explain the relatively small change in* H^- *and heavier anion yields from abasic tetramers* (Table 19-4).

The logic behind these assignments may also be seen by considering the branching ratios between electron emission into the continuum (e_c^-) and within DNA(e_t^-). These ratios depend on the magnitude of the departing electron wavefunction within

DNA and elsewhere. Owing to internal diffraction, the magnitude of the square of the electron wavefunction within DNA can be orders of magnitudes larger at very low energies. Thus, we expect the "electron transfer channel" to be strongly favored below ~4 eV; whereas at higher energies (e.g., at 9 eV), autoionization into the continuum should considerably increase. According to these decay channels, the anion yields can be produced locally via DEA (pathway 2) but also via pathway 1, as suggested for O^- and OH^- ESD from GCAT and its abasic configurations [90] and discussed in Section 19.6. In the energy range of core-excited resonances, however, diffraction is not very strong. Hence, the ESD signal does not exhibit a strong dependence upon the formation of abasic sites. On the other hand, in the case of pathway 3 the departing electron has a much lower energy, so that the amplitude of the reemitted electron wave becomes highly sensitive to the molecular arrangement of the oligonucleotide, and thus strongly influences the branching ratios between electron decay in the continuum and within DNA. At low energy, constructive interference favors electron residence within DNA. But when electron coherence is destroyed within DNA by molecular rearrangement following creation of an abasic site, electron emission in the continuum is considerably increased followed by a corresponding decrease in bond scission and base release.

Finally, adding water to DNA modifies transient anion states and increases damage. When water is condensed on the tetramer GCAT, anion ESD yield functions are modified in magnitude and line shapes. These changes are induced by the formation of new dissociative transient anions, which arise from the interaction between H_2O and DNA. The magnitude of ESD yields is increased by a factor of about 1.6 with 60% of the first hydration layer added to vacuum-dried DNA. Although the magnitude of this enhancement is significant, it is much smaller then the modification in various yields of products caused by the first hydration layer of DNA during the radiochemical events [1] that follow the deposition of the energy of LEE in irradiated cells.

ACKNOWLEDGEMENT

This work is financed by the Canadian Institutes of Health Research (CIHR). The author would like to thank Ms Francine Lussier for her skilled assistance in the preparation of this manuscript and Drs Andrew Bass and Marc Michaud for helpful suggestions and corrections.

ABBREVIATIONS

A Adenine
AL Attenuation lengths
C Cytosine
CL Crosslinks

d	Deoxyribose
DD	Dipolar dissociation
DEA	Dissociative electron attachment
DNA	Deoxyribonucleic acid
ds	Double strand
DSB	Double strand break(s)
ESD	Electron stimulated desorption
eV	Electron volts
G	Guanine
HPLC	High performance Liquid chromatography
HREEL	High resolution electron energy loss
keV	Kilo electron volts
LEE	Low energy electron(s) (0–30 eV)
LEEEF	Low energy electron enhancement factor
MFP	Mean free path(s)
ML	Monolayer(s)
p	Phosphate
MS	Mass spectrometry
SAM	Self assembled monolayer(s)
SB	Strand breaks
SE	Secondary electron(s)
ss	single strand
SSB	Single strand break(s)
SU	Subunit
T	Thymine
THF	Tetrahydrofuran
UHV	Ultra high vacuum
UV	Ultraviolet

REFERENCES

1. von Sonntag C (1987) The Chemical Basis for Radiation Biology, Taylor and Francis, London.
2. Ward JF (1977) Advances in Radiation Biology 5, Academic Press, New York.
3. Yamamoto O (1976) Aging, Carcinogenesis and Radiation Biology, Smith K (ed), Plenum, New York.
4. Fuciarelli AF, Zimbrick JD (eds) (1995) Radiation Damage in DNA: Structure/Function Relationships at Early Times, Batelle, Columbus.
5. Sanche L (2005) Eur Phys J D 35:367.
6. Cai Z, Cloutier P, Hunting D, Sanche L (2005) J Phys Chem B 109:4796.
7. International Commission on Radiation Units and Measurements (1979) ICRU Report 31, ICRU, Washington.
8. LaVerne JA, Pimblott SM (1995) Radiat Res 141:208.
9. Cobut V, Frongillo Y, Patau JP, Goulet T, Fraser M-J, Jay-Gerin J-P (1998) Radiat Phys Chem 51:229.
10. Bartels DM, Cook AR, Mudaliar M, Jonah CD (2000) J Phys Chem A 104:1686.

11. Barrios R, Skurski P, Simons J (2002) J Phys Chem B 10:7991.
12. Berdys J, Anusiewicz I, Skurski P, Simons J (2004) J Am Chem Soc 126:6441.
13. (a) Berdys J, Anusiewicz I, Skurski P, Simons J (2004) J Phys Chem A 108:2999; (b) Berdys J, Skurski P, Simons JJ (2004) Phys Chem B 108:5800.
14. Dabkowska I, Rak J, Gutowski M (2005) Eur Phys J D 35:429.
15. Gu J, Xie Y, Schaefer HF III (2006) Chem Phys Chem 7:1885.
16. Adams RLP, Knowler JT, Leader DP (1981) The Biochemistry of the Nucleic Acids, 10th edn. Chapman and Hall, New York.
17. Swarts S, Sevilla M, Becker D, Tokar C, Wheeler K (1992) Radiat Res 129:333.
18. Boudaïffa B, Cloutier P, Hunting D, Huels MA, Sanche L (2002) Radiat Res 157:227.
19. Porter MD, Bright TB, Allara DL, Chidsey CED (1987) J Am Chem Soc 109:3559.
20. Dugal P, Huels MA, Sanche L (1999) Radiat Res 151:325.
21. Dugal P, Abdoul-Carime H, Sanche L (2000) J Phys Chem B 104:5610.
22. Abdoul-Carime H, Dugal PC, Sanche L (2000) Radiat Res 153:23.
23. Kimball Physics Inc., ELG-2 electron gun, http://www.kimphys.com.
24. Nagesha K, Gamache J, Bass AD, Sanche L (1997) Rev Sci Instrum 68:3883.
25. Marsolais RM, Deschênes M, Sanche L (1989) Rev Sci Instrum 60:2724.
26. Meesungnoen J, Jay-Gerin J-P, Filali-Mouhim A, Mankhetkorn S (2002) Radiat Res 158:657.
27. Zheng Y, Cloutier P, Wagner JR, Sanche L (2004) Rev Sci Instrum 75:4534.
28. Kimmel GA, Orlando TM (1995) Phys Rev Lett 75:2606.
29. Abdoul-Carime H, Dugal PC, Sanche L (2000) Surf Sci 451:102.
30. Sanche L (1995) Scanning Microscopy 9:619.
31. Boudaiffa B, Cloutier P, Hunting D, Huels MA, Sanche L (2000) Science 287:1658.
32. Mott NF, Massey HSW (1965) The Theory of Atomic Collisions, Clarendon, Oxford.
33. Schulz GJ (1973) Rev Mod Phys 45:378, 423.
34. Allan M (1989) J Electr Spectr Rel Phenom 48:219.
35. Sanche L (1991) Excess Electrons in Dielectric Media, Jay-Gerin J-P and Ferradini C (eds), CRC Press, Boca Raton.
36. Christophorou LG (1984) Electron-Molecule Interactions and Their Applications, Academic Press, Orlando.
37. Massey HSW (1976) Negative Ions, University Press, London.
38. Palmer RE, Rous P (1992) Rev Mod Phys 64:383.
39. Sanche L (2000) Surf Sci 451:82.
40. Folkard M, Prise KM, Vojnovic B, Davies S, Roper MJ, Michael BD (1993) Int J Radiat Biol 64:651.
41. Boudaïffa B, Cloutier P, Hunting D, Huels MA, Sanche L (2000) Méd Sci 16:1281.
42. Huels MA, Boudaïffa B, Cloutier P, Hunting D, Sanche L (2003) J Am Chem Soc 125:4467.
43. Boudaiffa B, Hunting DJ, Cloutier P, Huels MA, Sanche L (2000) Int J Radiat Biol 76:1209.
44. Bass AD, Parenteau L, Huels MA, Sanche L (1998) J Chem Phys 109:8635.
45. Huels MA, Parenteau L, Sanche L (1997) Chem Phys Lett 279:223.
46. Sieger MT, Simpson WC, Orlando TM (1998) Nature 394:554.
47. Pan X, Cloutier P, Hunting D, Sanche L (2003) Phys Rev Lett 90:208102-1–208102-4.
48. Abdoul-Carime H, Cloutier P, Sanche L (2001) Radiat Res 155:625.
49. Pan X, Abdoul-Carime H, Cloutier P, Bass AD, Sanche L (2005) Radiat Phys Chem 72:193.
50. Antic D, Parenteau L, Lepage M, Sanche L (1999) J Phys Chem 103:6611.
51. Ptasiñska S, Denifl S, Grill V, Märk TD, Scheier P, Gohlke S, Huels MA, Illenberger E (2005) Angew Chem Int Ed 44:1657.
52. Martin F, Burrow PD, Cai Z, Cloutier P, Hunting DJ, Sanche L (2004) Phys Rev Lett 93:068101.

53. Aflatooni K, Gallup GA, Burrow PD (1998) J Phys Chem A 102:6205.
54. Panajotovic R, Martin F, Cloutier P, Hunting DJ, Sanche L (2006) Radiat Res 165:452.
55. Cai Z, Cloutier P, Hunting D, Sanche L (2006) Radiat Res 165:365.
56. Henke BL, Knauer JP, Premaratne K (1981) J Appl Phys 52:1509.
57. Henke BL, Smith JA, Attwood DT (1977) J Appl Phys 48:1852.
58. Pan X, Sanche L (2005) Phys Rev Lett 94:198104.
59. Crewe AV, Isaacson M, Johnson D (1971) Nature 231:262.
60. Herve du Penhoat MA, Huels MA, Cloutier P, Jay-Gerin JP, Sanche L (2001) J Chem Phys 114:5755.
61. Abdoul-Carime H, Sanche L (2001) Radiat Res 156:151.
62. Abdoul-Carime H, Sanche L (2002) Int J Radiat Biol 78:89.
63. Cai Z, Dextraze M-E, Cloutier P, Hunting D, Sanche L (2006) J Chem Phys 124:024705.
64. Petrovykh DY, Kimura-Suda H, Tarlov M J, Whitman LJ (2004) Langmuir 20:429.
65. Ray SG, Daube SS, Naaman R (2005) PNAS 102:15.
66. Aqua T, Naaman R, Daube SS (2003) Langmuir 19:10573.
67. Pan X, Sanche L (to be published).
68. Huels MA, Parenteau L, Sanche L (2004) J Phys Chem B 108:16303.
69. Zheng Y, Cloutier P, Hunting DJ, Sanche L, Wagner JR (2005) J Am Chem Soc 127:16592.
70. Zheng Y, Cloutier P, Hunting DJ, Wagner JR, Sanche L (2006) J Chem Phys 124:64710.
71. Zheng Y, Wagner R, Sanche L (2006) Phys Rev Lett 96:208101.
72. Zheng Y, Cloutier P, Hunting DJ, Wagner JR, Sanche L (2004) J Am Chem Soc 126:1002.
73. Abdoul-Carime H, Gohlke S, Fischbach E, Scheike J, Illenberger E (2004) Chem Phys Lett 387:267.
74. Becker D, Bryant-Friedrich A, Trzasko C, Sevilla MD (2003) Radiat Res 160:174.
75. Becker D, Razskazovskii Y, Callaghan M, Sevilla MD (1996) Radiat Res 146:361.
76. Shukla L, Pazdro R, Becker D, Sevilla MD (2005) Radiat Res 163:591.
77. Range K, McGrath MJ, Lopez X, York DM (2004) J Am Chem Soc 126:1654.
78. Rowntree P, Sambe H, Parenteau L, Sanche L (1993) Phys Rev B 47:4537.
79. Hotop H, Ruf MW, Llan M, Fabrikant II (2003) Adv Atom Mol Opt Phys 49:85.
80. Berdys J, Anusiewicz I, Skurski P, Simons J (2004) J Am Chem Soc 125:6551.
81. Lévesque PL, Michaud M, Cho W, Sanche L (2005) J Chem Phys 122:224704.
82. Winstead C, McKoy V (2007) Phys Rev Lett 98:113201.
83. Caron LG, Sanche L (2003) Phys Rev Lett 91:113201; (2004) Phys Rev A 70:032719; (2005) 72:32726.
84. Pan X, Sanche L (2006) Chem Phys Lett 421:404.
85. Solomun T, Illenberger E (2004) Chem Phys Lett 396:448.
86. Solomun T, Hultschig C, Hultschig C, Illenberger E (2005) Eur Phys J D 35:437.
87. Tanabe T, Noda K, Saito M, Starikov EB, Tateno M (2004) Phys Rev Lett 93:043201.
88. Ladik J, Fruechtl H, Otto P, Jäger J (1993) J Mol Struct 297:215.
89. Ptasiñska S, Sanche L (2006) J Chem Phys 125:144713.
90. Ptasiñska S, Sanche L (2007) Phys Chem Chem Phys 14:1730.
91. Ptasiñska S, Sanche L (2007) Phys Rev E 75:031915.
92. Abdoul-Carime H, Langer J, Huels MA, Illenberger E (2005) Eur Phys J D 35:399.
93. Denifl S, Ptasiñska S, Probst M, Hrušák J, Scheier P, Märk TD (2004) J Phys Chem A 108:6562.
94. Denifl S, Ptasiñska S, Cingel M, Matejcik S, Scheier P, Märk TD (2003) Chem Phys Lett 377:74.
95. Ptasiñska S, Denifl S, Gohlke S, Scheier P, Illenberger E, Märk TD (2006) Angew Chem Int Ed 45:1893.

96. Burrow PD, Gallup GA, Scheer AM, Denifl S, Ptasiñska S, Märk TD, Scheier P (2006) J Chem Phys 124:124310.
97. Denifl S, Zappa F, Mähr I, Lecointre J, Probst M, Märk TD, Scheier P (2006) Phys Rev Lett 97:043201.
98. Hubert D, Beikircher M, Denifl S, Zappa F, Matejcik S, Bacher A, Grill V, Märk TD, Scheier P (2006) J Chem Phys 125:084304.
99. Ptasiñska S, Denifl S, Grill V, Märk TD, Illenberger E, Scheier P (2005) Phys Rev Lett 95:093201.
100. Ptasiñska S, Denifl S, Mróz B, Brobst M, Grill V, Illenberger E, Scheier P, Märk TD (2005) J Chem Phys 123:124302.
101. Sulzer P, Ptasiñska S, Zappa F, Mielewska B, Milosavljevic AR, Scheier P, Mark TD, Bald I, Gohlke S, Huels MA, Illenberger E (2006) J Chem Phys 125:044304.
102. Abdoul-Carime H, Gohlke S, Illenberger E (2004) Phys Rev Lett 92:168103.
103. Ptasiñska S, Denifl S, Scheier P, Illenberger E, Märk TD (2005) Angew Chem Int Ed 44:6941.
104. Caron LG, Sanche L (2005) Phys Rev A 72:032726.
105. Caron LG, Sanche L (2006) Phys Rev A 73:062707.
106. Tao NJ, Lindsay SM (1989) Biopolymers 28:1019.
107. Simpson WC, Sieger MT, Orlando T, Parenteau L, Naghesha K, Sanche L (1997) J Chem Phys 107:8668.
108. Casaes RN, Paul JB, McLaughlin RP, Saykally RJ, van Mourik T (2004) J Phys Chem A 108:10989; Choi MY, Miller RE (2005) Phys Chem Chem Phys 7:3565.
109. Whitson KB, Lukan AM, Marlowe RL, Lee SA, Anthony L, Rupprecht A (1998) Phys Rev E 58:2370; Cavanaugh D, Lee SA (2002) J Biomol Struct Dyn 19:709.
110. Gu J, Wang J, Lesczynski J (2006) J Am Chem Soc 128:322.
111. Li X, Sevilla MD, Sanche L (2003) J Am Chem Soc 125:3668.
112. Dabkowska I, Rak J, Gutowski M (2005) Eur Phys J D 35:29.